

Error Floor Analysis of LDPC Row Layered Decoders

Ali Farsiabi and Amir H. Banihashemi, *Senior Member, IEEE*

Abstract

In this paper, we analyze the error floor of quasi-cyclic (QC) low-density parity-check (LDPC) codes decoded by the sum-product algorithm (SPA) with row layered message-passing scheduling. For this, we develop a linear state-space model of trapping sets (TSs) which incorporates the layered nature of scheduling. We demonstrate that the contribution of each TS to the error floor is not only a function of the topology of the TS, but also depends on the row layers in which different check nodes of the TS are located. This information, referred to as TS layer profile (TSLP), plays an important role in the harmfulness of a TS. As a result, the harmfulness of a TS in particular, and the error floor of the code in general, can significantly change by changing the order in which the information of different layers, corresponding to different row blocks of the parity-check matrix, is updated. We also study the problem of finding a layer ordering that minimizes the error floor, and obtain row layered decoders with error floor significantly lower than that of their flooding counterparts. As part of our analysis, we make connections between the parameters of the state-space model for a row layered schedule and those of the flooding schedule. Simulation results are presented to show the accuracy of analytical error floor estimates.

Index Terms

LDPC codes, QC-LDPC codes, layered decoding, row layered decoding, message-passing schedule, layered schedule, row layered schedule, horizontal layered schedule, error floor, low error floor, error floor analysis, linear state-space model, trapping sets (TS), elementary TSs (ETS), leafless elementary TSs (LETS).

I. INTRODUCTION

Finite-length low-density parity-check (LDPC) codes under iterative message passing algorithms suffer from error floor, i.e., as the channel quality improves, at some point, the error rate does not decrease as fast as its initial rate of decrease. The error floor problem of LDPC codes

has been the topic of extensive research in recent years. In [1]–[10], decoders with improved error floor were devised. For quantized message-passing decoders, it is well-known that clipping messages, in general, causes an error floor [11]. The error floor generally worsens as the dynamic range of messages is reduced [7]. Different techniques to improve the error floor by adjusting the dynamic range of (some of) the messages were presented in [6], [7], [9]. LDPC codes with low error floor were constructed in [12]–[26]. Characterization and enumeration of structures responsible for error floor were studied in [27]–[32], and techniques to estimate the error floor were developed in [33]–[50].

There are two general categories of techniques to estimate the error floor of LDPC codes. The first category is based on importance sampling techniques, and requires the full knowledge of the parity-check matrix or Tanner graph of the code to estimate the error floor [33], [35]–[39], [41], [43]. The second category, on the other hand, is code-independent, in that, rather than the full knowledge of the code’s Tanner graph, these techniques only require the multiplicity and topology of harmful substructures of the Tanner graph, referred to as *trapping sets* (TSs), and possibly the degree distributions of the graph, to estimate the error floor [34], [40], [42], [45]–[47], [51]. In particular, in [34], [42], [45], to evaluate the performance of an LDPC code over the additive white Gaussian noise (AWGN) channel, a linear state-space model is used to represent the dynamics of the sum-product algorithm (SPA) in the vicinity of a TS of interest with the inputs to the model generated using density evolution (DE) [52]. Based on this model, the failure probability of the TS, which is only a function of the topology of the TS and the degree distribution of the Tanner graph, is calculated. The error floor is then estimated as a weighted sum of these failure probabilities over dominant TSs of the code, with the weights being the multiplicities of different TS structures.

Among TSs, the most harmful ones are those with only degree-1 and degree-2 check nodes in their induced subgraphs [3], [53]. Such TSs are called *elementary* (ETS). The degree-1 and degree-2 check nodes are referred to as *unsatisfied* and *missatisfied* check nodes, respectively. In [34], Sun proposed a linear state-space model to analyze the dynamics of ETSs in the error floor region over the AWGN channel. This model was based on the assumption that the decoder behavior outside an ETS can be well approximated by DE. Schlegel and Zhang [42] proposed an improved linear state-space model in which an iteration-dependent linear gain was added to the model to account for the impact of external messages of missatisfied check nodes on the internal messages of an ETS. More recently, Butler and Siegel [45] refined and extended the linear state-

space model and used it to analyze the effect of log-likelihood ratio (LLR) saturation on the error floor performance of LDPC codes with fixed variable-node degrees decoded by floating-point SPA.

To the best of our knowledge, all the existing work on the theoretical analysis of error floor, including [34], [42], [45], is limited to two-phase message passing algorithms, also known as *flooding* or *parallel schedule*. In flooding schedule, each decoding iteration is divided into two parts. In the first (second) part of an iteration, all the variable (check) nodes compute their messages and pass them to their adjacent check (variable) nodes simultaneously. There are however a variety of message passing schedules which are advantageous to flooding in terms of performance, complexity or convergence speed [54]–[66]. An important category of schedules are *layered* or *serial schedules* [54], [55], [60], [61], [63], [64]. In such schedules, each iteration of message-passing consists of multiple sub-iterations performed serially. This allows a more frequent updating of the reliabilities in each iteration compared to the flooding schedule, which consequently results in a higher convergence speed. Moreover, due to the reuse of the same hardware for the implementation of different sub-iterations, the hardware resources required for the implementation of layered decoders are substantially lower than those of their flooding counterparts. Due to these attractive features, layered decoders are often used in practical applications along with quasi-cyclic (QC) LDPC codes. In such a combination, the row or column blocks of the parity-check matrix of the QC-LDPC code correspond to different layers. The layered decoder is then referred to as *row (horizontal) layered decoder* [54], [55], [58], [60], [62], [63] or *column (vertical) layered decoder* [64], respectively. In [61], it has been shown that the convergence speed of both types of layered decoder can be twice that of a decoder with flooding schedule.

The vast majority of research on layered decoders is devoted to the issues concerning convergence speed and efficient implementations. In particular, the study of the error floor of such decoders has been mainly limited to empirical results [65]–[70]. In [65] and [66], the authors proposed a dynamic scheduling and a schedule diversity, respectively, that reduced the error floor. More recently, Raveendran and Vasic [67] studied flooding and row layered Gallager-B algorithms applied to the $(155, 64)$ Tanner code over the binary symmetric channel, and demonstrated that while the former decoder gets trapped in $(5, 3)$ ETSs, the latter does not, and as a result the layered decoder has a superior error floor performance compared to the flooding decoder.

Motivated by the wide spread application of layered decoders and the fact that the behavior of such decoders in the error floor region is still not well understood, in this paper, we aim at the theoretical analysis of the error floor of row layered decoders. In fact, to the best of our knowledge, this is the first work in which the dynamics of a soft layered decoder in the error floor region is theoretically analyzed. We start by developing a linear state-space model for ETSs that incorporates the layered nature of the decoding algorithm. We then use this model to study the dynamics of a saturating SPA in the vicinity of the TS over the AWGN channel. Our analysis shows that the harmfulness of a given TS, as well as the error floor of the code, can significantly change by changing the order in which the information of different layers, corresponding to different row blocks of the parity-check matrix, are updated.¹ We then study the problem of finding the layer ordering that minimizes the error floor. As a result, we find orderings that result in error floors substantially lower than those of the decoder with flooding schedule. Connections are also made between the model parameters of the layered decoder and those of the flooding one. Finally, we compare our theoretical estimates of the error floor with Monte Carlo simulations for QC-LDPC codes, both variable-regular and irregular, and demonstrate a good match between the two.

The rest of the paper is organized as follows: In Section II, we present some preliminaries. This is followed by a review of the linear state-space model of an ETS for a decoder with the flooding schedule in Section III. We then develop the linear state-space model of an ETS for a row layered decoder in Section IV. In the same section, we also establish connections between the model parameters of the row layered and flooding schedules. In Section V, we analyze the effect of different row block permutations on some important parameters affecting the error floor performance of the layered decoder, and discuss the optimization of the layer ordering to minimize the error floor. In Section VI, we present the simulation results to evaluate the accuracy of the theoretical results in estimating the error floor. We end the paper with some concluding remarks in Section VII.

¹Our experiments show that the waterfall performance of the codes is rather insensitive to the updating order of layers.

II. PRELIMINARIES

A. Notations

In this paper, matrices and vectors are denoted by boldfaced upper case and lower case letters, respectively. The only exceptions are the LLR vectors where the symbol \mathbf{L} with different subscripts or superscripts is utilized for representation. All the vectors are assumed to be column vectors. A list of the notations and symbols used in this paper is provided in Tables I and II.

B. LDPC codes, SPA, flooding and layered schedules and TSs

Consider a binary LDPC code \mathcal{C} with parity-check matrix \mathbf{H} . A codeword of \mathcal{C} is denoted by \mathbf{d} , and satisfies $\mathbf{H}\mathbf{d} = \mathbf{0}$. Let $G = (V \cup C, E)$ be the Tanner graph representing \mathcal{C} , where $V = \{v_1, v_2, \dots, v_n\}$ and $C = \{c_1, c_2, \dots, c_m\}$ are the sets of variable nodes (VNs) and check nodes (CNs), respectively, and $E = \{e_1, e_2, \dots, e_k\}$ is the set of edges. Suppose that \mathcal{C} is used for transmission over an AWGN channel using a binary phase shift keying (BPSK) modulation, where codeword bits d_i are mapped to modulated symbols $u_i = (-1)^{d_i}$. At the channel output, we thus have $y_i = u_i + n_i$, where $\{n_i\}$ represents the noise and is a zero-mean Gaussian random process with independent and identically distributed (i.i.d.) values, each with variance σ_{ch}^2 .

For decoding, we assume SPA is used with the following channel LLR values as the input:

$$L_i^{ch} = 2y_i/\sigma_{ch}^2. \quad (1)$$

The message sent from VN v_i to CN c_j at iteration ℓ is given by

$$L_\ell^{[i \rightarrow j]} = L_i^{ch} + \sum_{k \in M(i) \setminus j} L_{\ell-1}^{[i \leftarrow k]}, \quad (2)$$

where $M(i) \setminus j$ represents the set of CNs adjacent to VN v_i excluding c_j , and $L_{\ell-1}^{[i \leftarrow k]}$ denotes the message sent from CN c_k to VN v_i at iteration $\ell - 1$. At the first iteration of the algorithm, all the messages sent from check nodes to variable nodes at iteration $\ell - 1$ are assumed to be zero in (2). The CN to VN messages in SPA are computed as

$$L_\ell^{[i \leftarrow j]} = 2 \tanh^{-1} \left[\prod_{k \in N(j) \setminus i} \tanh \frac{L_\ell^{[k \rightarrow j]}}{2} \right], \quad (3)$$

where $N(j) \setminus i$ represents the set of VNs adjacent to CN c_j excluding v_i . At the end of each iteration, for each $i \in \{1, \dots, n\}$, first, the total LLR is calculated by

$$\tilde{L}_\ell^{[i]} = L_i^{ch} + \sum_{k \in M(i)} L_\ell^{[i \leftarrow k]}, \quad (4)$$

TABLE I
NOTATIONS AND SYMBOLS (PART A)

Notations	Descriptions
\mathbf{H}	$m \times n$ parity check matrix
\mathbf{H}_b	$m_b \times n_b$ base matrix
\mathbf{d}	A codeword
$\hat{\mathbf{d}}$	Estimated codeword
I_{max}	Maximum number of iterations
L_i^{ch}	Channel LLR
$L_\ell^{[i \leftarrow j]}$	j th CN to i th VN message at iteration ℓ
$L_\ell^{[i \rightarrow j]}$	i th VN to j th CN message at iteration ℓ
$\tilde{L}_\ell^{[i]}$	Total LLR of i th VN at iteration ℓ
m_s	Number of state variables
\mathcal{S}	Set of VNs of a TS, $ \mathcal{S} = a$
$\Gamma(\mathcal{S})$	Set of CNs of a TS
$\Gamma_o(\mathcal{S})$	Set of odd-degree CNs of a TS, $ \Gamma_o(\mathcal{S}) = b$
$\Gamma_e(\mathcal{S})$	Set of even-degree CNs of an ETS, $ \Gamma_e(\mathcal{S}) = \frac{m_a}{2}$
$\mathbf{x}^{(\ell)}$	$m_s \times 1$ state vector of a LETS in flooding decoder at the ℓ th iteration
\bar{g}_ℓ	Missatisfied CN multiplicative gains in flooding decoder at the ℓ th iteration
\mathbf{A}	$m_s \times m_s$ transition matrix of a LETS in flooding decoder
\mathbf{B}	$m_s \times a$ matrix determining the channel input contributions to the state variables in flooding decoder
\mathbf{B}_{ex}	$m_s \times b$ matrix determining the contribution of unsatisfied CN inputs to state variables in flooding decoder
\mathbf{C}	$a \times m_s$ matrix determining the relation of state variables with the total LLR vector
\mathbf{D}_{ex}	$a \times b$ matrix determining the contribution of unsatisfied CN inputs to the total LLR vector
\mathbf{L}	$a \times 1$ channel input vector in the LETS linear model
$\mathbf{L}_{ex}^{(\ell)}$	$b \times 1$ unsatisfied CN input vector in the LETS linear model at the ℓ th iteration
$\tilde{\mathbf{L}}^{(\ell)}$	$a \times 1$ total LLR vector in the LETS linear model
\mathbf{P}	A permutation matrix
$\rho(\mathbf{M})$	Spectral radius of a matrix \mathbf{M}
r	Dominant eigenvalue of the flooding transition matrix \mathbf{A}
$\mathbf{w}_1^T, \mathbf{u}_1$	Left and right eigenvectors corresponding to r
\mathbb{C}	Set of complex numbers
β'_ℓ	Error indicator function of flooding decoder
$P_e\{\mathcal{S}\}$	Probability of failure of TS \mathcal{S}
L_i	i th row layer of a QC-LDPC code
J	Number of missatisfied CN layers in a TS
$(\cdot)_k$	k th element of a vector
(m_{ch}, σ_{ch}^2)	Mean and variance of the channel noise
$(m_{ex}^{(\ell)}, \sigma_{ex}^{(\ell)})$	Mean and variance of the unsatisfied CN inputs at iteration ℓ of the flooding decoder

TABLE II
NOTATIONS AND SYMBOLS (PART B)

Notations	Descriptions
n_{L_j}	Number of state variables of a LETS within layer j
\mathcal{A}_j	$m_s \times m_s$ transition matrix of layer j
\mathcal{B}_j	$m_s \times a$ matrix indicating the contribution of the channel LLRs in the calculation of the state variables of the j th layer
$\overset{\triangleleft}{\mathcal{B}}_{ex,j}, \overset{\triangleright}{\mathcal{B}}_{ex,j}$	$m_s \times b$ matrices indicating the contribution of $\mathbf{L}_{ex}^{(\ell-1)}$ and $\mathbf{L}_{ex}^{(\ell)}$ in updating the state variables within the j th layer
$\mathbf{G}^{(\ell)}$	$m_s \times m_s$ matrix whose diagonal entries are the gains corresponding to the m_s state variables
$\mathcal{G}_j^{(\ell)}$	$m_s \times m_s$ gain matrix corresponding to the j th layer of iteration ℓ
$\tilde{\mathbf{x}}^{(\ell,j)}$	Layered decoder state vector of layer j at iteration ℓ
$\tilde{\mathbf{B}}^{(\ell)}$	$m_s \times a$ matrix indicating the contribution of the channel LLRs in calculation of the state variables at the ℓ th iteration of the layered decoder
$\overset{\triangleleft}{\mathbf{B}}_{ex}^{(\ell)}, \overset{\triangleright}{\mathbf{B}}_{ex}^{(\ell)}$	$m_s \times b$ matrices illustrating the contribution of $\mathbf{L}_{ex}^{(\ell-1)}$ and $\mathbf{L}_{ex}^{(\ell)}$ in updating the state variables at the ℓ th iteration of the layered decoder
$\hat{\psi}_\ell^{[k' \rightarrow j]}$	Probability distribution of the messages from virtual VN $v_{k'}$ to missatisfied CN c_j at iteration ℓ
$P_{inv,\ell}^{[k' \rightarrow j]}$	Probability of polarity inversion in the messages from virtual VN $v_{k'}$ to missatisfied CN c_j at iteration ℓ
$\bar{g}_{c_j}^{(\ell)}, \tilde{g}_{c_j}^{(\ell)}$	Average gains of missatisfied CN c_j at the ℓ th iteration of layered decoder before and after adding the polarity inversion, respectively
$\tilde{\mathbf{A}}_{J \rightarrow 1}$	Transition matrix of a LETS with J layers in layered decoding
\tilde{r}	Dominant eigenvalue of $\tilde{\mathbf{A}}_{J \rightarrow 1}$
$\tilde{\mathbf{w}}_1^T, \tilde{\mathbf{u}}_1$	Left and right eigenvectors corresponding to \tilde{r}
$\tilde{\mathbf{A}}$	The only irreducible diagonal block of the Frobenius normal form of $\tilde{\mathbf{A}}_{J \rightarrow 1}$ for LETSs that are not simple cycles
$\tilde{\omega}_1^T, \tilde{\nu}_1$	Dominant left and right eigenvectors of $\tilde{\mathbf{A}}$
D_l	A LETS digraph of the layered decoder with nodes V_l and edges E_l
D_f	A LETS digraph of the flooding decoder with nodes V_f and edges E_f
n_z	Number of zero columns of the transition matrix of the layered decoder
$(\mathbf{m}_{ex}^{(\ell)}, \mathbf{\Sigma}_{ex}^{(\ell)})$	$b \times 1$ mean vector and $b \times b$ covariance matrix of the inputs from unsatisfied CNs of a LETS at iteration ℓ
$\tilde{\beta}^{(\ell)}$	Error indicator function of layered decoder
Υ_i	Size of the i th TS group
Π_J	Set of all the $J!$ permutations of the layers of a LETS
$\overleftarrow{\psi}_\ell^j$	Average distribution of CN to VN messages at layer j of iteration ℓ
$\overrightarrow{\psi}_\ell^j$	Average distribution of VN to CN messages at layer j of iteration ℓ

and then, a hard decision is made by

$$\hat{d}_i = [\text{sign}(\tilde{L}_\ell^{[i]}) + 1]/2. \quad (5)$$

If the decoded block, $\hat{\mathbf{d}}$, at the end of iteration $\ell \leq I_{max}$, is a codeword, i.e., if $\mathbf{H}\hat{\mathbf{d}} = \mathbf{0}$, then the decoding is terminated successfully. (I_{max} is the maximum number of iterations.) Otherwise, if iteration I_{max} is completed and still no codeword is found, then a decoding failure is declared.

To circumvent the numerical errors in the calculation of $\tanh(x)$ in (3), similar to [7], [71], we use the following equivalent operation to calculate CN to VN messages:

$$L_\ell^{[i \leftarrow j]} = \boxplus_{k \in N(j) \setminus i} L_\ell^{[k \rightarrow j]}, \quad (6)$$

in which the pairwise box-plus operator, \boxplus , is defined as

$$\begin{aligned} x_1 \boxplus x_2 &= \ln \left(\frac{1 + e^{x_1 + x_2}}{e^{x_1} + e^{x_2}} \right) \\ &= \text{sign}(x_1)\text{sign}(x_2) \cdot \min(|x_1|, |x_2|) + s(x_1, x_2). \end{aligned} \quad (7)$$

The term $s(x_1, x_2)$ in (7) is given by

$$s(x_1, x_2) = \ln \left(1 + e^{-|x_1 + x_2|} \right) - \ln \left(1 + e^{-|x_1 - x_2|} \right). \quad (8)$$

It should be noted that Equations (2), (3), and (6) are edgewise operations, and can thus be executed within various scheduling frameworks. In decoders with *flooding schedule*, at the first half of each iteration, Equation (2) is executed for all the VN to CN messages. In the second half of the iteration, all the CN to VN messages are updated based on (3). For decoders with *row layered schedule*, the CNs are partitioned into different subgroups (layers). Within each CN subgroup, messages are only generated on the edges between the CNs in the subgroup and their adjacent VNs while the other edges in the graph remain inactive. After the messages within a subgroup are generated, the updated reliabilities are used in the following layers. In Algorithm 1, the steps of the row layered SPA is presented for a QC-LDPC code. In this paper, we consider QC-LDPC codes whose parity-check matrices \mathbf{H} consist of an $m_b \times n_b$ array of circulant permutation matrices (CPMs) of size $p \times p$ and zero matrices of the same size. The Tanner graph of such codes can be considered as a cyclic p -lifting of a bipartite *base graph* with n_b VNs and m_b CNs. Each layer of the row layered decoder in this case corresponds to one row block of \mathbf{H} , and thus, there are m_b layers. It should be noted that the equation in Line 7 of Algorithm 1 is derived by combining (2) and (4). As can be seen, the total LLR of each

VN may be updated several times within an iteration. So, for simplicity, the iteration index, ℓ , is removed from the symbol $\tilde{L}^{[i]}$.

Algorithm 1 Row Layered Box-Plus Decoding Algorithm

```

1: Input: Channel LLRs for all the VNs.
2: Initialization: All the total LLRs are initialized with the channel LLRs,  $\tilde{L}^{[i]} = L_i^{ch}$  for VNs
    $i = 1 : n_bp$ .
3: for iteration  $\ell = 1, \dots, I_{max}$  do
4:   for The CN group (layer) number  $z = 1 : m_b$  do
5:     for CNs  $j = (z - 1)p + 1, \dots, zp$ , in layer  $z$  do
6:       for all VNs  $i \in N(j)$  do
7:          $L_\ell^{[i \rightarrow j]} = \tilde{L}^{[i]} - L_{\ell-1}^{[i \leftarrow j]}$ .
8:       end for
9:       for all VNs  $i \in N(j)$  do
10:         $L_\ell^{[i \leftarrow j]} = \bigoplus_{k \in N(j) \setminus i} L_\ell^{[k \rightarrow j]}$ ,
11:         $\tilde{L}^{[i]} = L_\ell^{[i \rightarrow j]} + L_\ell^{[i \leftarrow j]}$ .
12:      end for
13:    end for
14:  end for
   Hard-decision:
15:  for all VNs  $i = 1, \dots, n_bp$  do
16:     $\hat{d}_i = [\text{sign}(\tilde{L}^{[i]}) + 1]/2$ .
17:  end for
18:  if  $\text{H}\hat{\mathbf{d}} = \mathbf{0}$  then
19:    Break.
20:  end if
21: end for
22: Output:  $\hat{\mathbf{d}}$ 

```

C. Trapping sets (TSs)

It is well-known that in the error floor region, the majority of the errors of iterative decoding algorithms occur as a result of the decoder getting trapped within a subset \mathcal{S} of VNs, i.e.,

although all the bits outside \mathcal{S} have correct values for sufficiently large number of iterations, all the bits inside \mathcal{S} are in error. In this case, the set \mathcal{S} is called a *trapping set (TS)*. Let \mathcal{S} be a TS, and $\Gamma(\mathcal{S})$ be the set of neighboring CNs of \mathcal{S} in the Tanner graph G . The *induced subgraph* of \mathcal{S} in G , denoted by $G(\mathcal{S})$, is a graph whose nodes and edges are $\mathcal{S} \cup \Gamma(\mathcal{S})$ and $\{v_i c_j \in E : v_i \in \mathcal{S}, c_j \in \Gamma(\mathcal{S})\}$, respectively. The set of CNs, $\Gamma(\mathcal{S})$, can be partitioned into even-degree CNs, $\Gamma_e(\mathcal{S})$, and odd-degree CNs, $\Gamma_o(\mathcal{S})$. The members of $\Gamma_o(\mathcal{S})$ and $\Gamma_e(\mathcal{S})$ are referred to as *unsatisfied check nodes* and *missatisfied check nodes*, respectively. If all the CNs in $\Gamma(\mathcal{S})$ have degrees 1 or 2, the TS is called an *elementary TS (ETS)*. An ETS \mathcal{S} is referred to as a *leafless ETS (LETS)* if each variable node in \mathcal{S} is connected to at least two missatisfied CNs. Leafless ETSs are known to be the most harmful TSs over the AWGN channel [45], [53]. Similar to [45], we thus limit our discussions in this paper to LETSs. In the rest of the paper, for simplicity, sometimes, we use the term “TS” instead of “LETS.”

Trapping sets are often identified by their size, $|\mathcal{S}| = a$, and the number of unsatisfied CNs in their subgraph, $|\Gamma_o(\mathcal{S})| = b$. In this case, the TS is said to belong to the (a, b) *class*, or is referred to as an (a, b) TS.

III. LINEAR STATE-SPACE MODEL OF LETSs FOR SPA WITH FLOODING SCHEDULE

A. The Model

The linear state-space model of a LETS is given by [45]

$$\mathbf{x}^{(0)} = \mathbf{B}\mathbf{L} \quad (9)$$

$$\mathbf{x}^{(\ell)} = \bar{g}'_{\ell} \mathbf{A} \mathbf{x}^{(\ell-1)} + \mathbf{B}\mathbf{L} + \mathbf{B}_{ex} \mathbf{L}_{ex}^{(\ell)}, \text{ for } \ell \geq 1, \quad (10)$$

$$\tilde{\mathbf{L}}^{(\ell)} = \bar{g}'_{\ell} \mathbf{C} \mathbf{x}^{(\ell-1)} + \mathbf{L} + \mathbf{D}_{ex} \mathbf{L}_{ex}^{(\ell)}, \text{ for } \ell \geq 1. \quad (11)$$

In the above equations, the vector $\mathbf{x}^{(\ell)}$ represents the state vector at iteration ℓ . The elements of this vector, called state variables, are the LLR messages passed over different edges of the LETS subgraph towards the missatisfied CNs. For an (a, b) LETS, the number of state variables is equal to $m_s = \sum_{i=1}^a d_{v_i} - b$, where d_{v_i} is the degree of the i th variable node in the LETS. The state variables are initialized in (9), and then updated in each iteration using (10). The relationship between state variables in consecutive iterations are established through the $m_s \times m_s$ matrix \mathbf{A} , referred to as the *transition matrix*. The model has two input vectors $\mathbf{L}_{ex}^{(\ell)}$ and \mathbf{L} with sizes b and a , respectively. The elements of these vectors are the messages from the unsatisfied (degree-one)

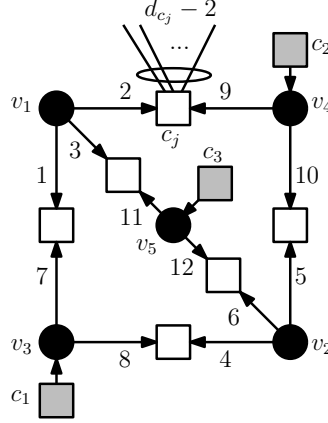


Fig. 1. A $(5, 3)$ LETS. The VNs, missatisfied CNs and unsatisfied CNs are shown by black circles, white squares and gray squares, respectively. The external connections for one of the missatisfied CNs are also shown.

CNs at iteration ℓ and the channel LLRs, respectively. Matrices \mathbf{B} and \mathbf{B}_{ex} are responsible for the contribution of channel LLRs and unsatisfied CN messages to state variables, respectively. The $a \times 1$ output vector $\tilde{\mathbf{L}}^{(\ell)}$ represents the total LLR values of the LETS variable nodes, given in (4). The contributions of the state variables and unsatisfied CN messages to this vector is accounted for through matrices \mathbf{C} and \mathbf{D}_{ex} , respectively. The parameter \bar{g}'_{ℓ} is a multiplicative gain to account for the effect of the external messages entering the missatisfied CNs. The calculation of \bar{g}'_{ℓ} is discussed later in Subsection III-C.

Example 1. In Fig. 1, the structure of $(5, 3)$ LETSs of Tanner $(155, 64)$ code is shown. The matrices in the linear state-space model for this LETS structure, corresponding to the edge and node labels in Fig. 1, are the followings:

$$\begin{aligned}
\mathbf{A} = & \begin{bmatrix} 0 & 0 & 0 & 0 & 0 & 0 & 0 & 0 & 1 & 0 & 1 & 0 \\ 0 & 0 & 0 & 0 & 0 & 0 & 1 & 0 & 0 & 0 & 1 & 0 \\ 0 & 0 & 0 & 0 & 0 & 0 & 1 & 0 & 1 & 0 & 0 & 0 \\ 0 & 0 & 0 & 0 & 0 & 0 & 0 & 0 & 0 & 1 & 0 & 1 \\ 0 & 0 & 0 & 0 & 0 & 0 & 0 & 1 & 0 & 0 & 0 & 1 \\ 0 & 0 & 0 & 0 & 0 & 0 & 0 & 1 & 0 & 1 & 0 & 0 \\ 0 & 0 & 0 & 1 & 0 & 0 & 0 & 0 & 0 & 0 & 0 & 0 \\ 1 & 0 & 0 & 0 & 0 & 0 & 0 & 0 & 0 & 0 & 0 & 0 \\ 0 & 0 & 0 & 0 & 1 & 0 & 0 & 0 & 0 & 0 & 0 & 0 \\ 0 & 1 & 0 & 0 & 0 & 0 & 0 & 0 & 0 & 0 & 0 & 0 \\ 0 & 0 & 0 & 0 & 0 & 1 & 0 & 0 & 0 & 0 & 0 & 0 \\ 0 & 0 & 1 & 0 & 0 & 0 & 0 & 0 & 0 & 0 & 0 & 0 \end{bmatrix}, \mathbf{B} = \begin{bmatrix} 1 & 0 & 0 & 0 & 0 \\ 1 & 0 & 0 & 0 & 0 \\ 1 & 0 & 0 & 0 & 0 \\ 0 & 1 & 0 & 0 & 0 \\ 0 & 1 & 0 & 0 & 0 \\ 0 & 1 & 0 & 0 & 0 \\ 0 & 0 & 1 & 0 & 0 \\ 0 & 0 & 1 & 0 & 0 \\ 0 & 0 & 0 & 1 & 0 \\ 0 & 0 & 0 & 1 & 0 \\ 0 & 0 & 0 & 0 & 1 \\ 0 & 0 & 0 & 0 & 1 \end{bmatrix}, \mathbf{B}_{ex} = \begin{bmatrix} 0 & 0 & 0 \\ 0 & 0 & 0 \\ 0 & 0 & 0 \\ 0 & 0 & 0 \\ 0 & 0 & 0 \\ 0 & 0 & 0 \\ 1 & 0 & 0 \\ 1 & 0 & 0 \\ 0 & 1 & 0 \\ 0 & 1 & 0 \\ 0 & 0 & 1 \\ 0 & 0 & 1 \end{bmatrix}, \\
\mathbf{C} = & \begin{bmatrix} 0 & 0 & 0 & 0 & 0 & 0 & 1 & 0 & 1 & 0 & 1 & 0 \\ 0 & 0 & 0 & 0 & 0 & 0 & 0 & 1 & 0 & 1 & 0 & 1 \\ 1 & 0 & 0 & 1 & 0 & 0 & 0 & 0 & 0 & 0 & 0 & 0 \\ 0 & 1 & 0 & 0 & 1 & 0 & 0 & 0 & 0 & 0 & 0 & 0 \\ 0 & 0 & 1 & 0 & 0 & 1 & 0 & 0 & 0 & 0 & 0 & 0 \end{bmatrix}, \mathbf{D}_{ex} = \begin{bmatrix} 0 & 0 & 0 \\ 0 & 0 & 0 \\ 1 & 0 & 0 \\ 0 & 1 & 0 \\ 0 & 0 & 1 \end{bmatrix}.
\end{aligned}$$

As an example, the first row of matrix \mathbf{A} has a '1' in columns 9 and 11. By (10), this means that the first state variable (x_1) at iteration ℓ is a function of state variables x_9 and x_{11} at iteration $\ell - 1$. This relationship between the state variables at consecutive iterations can also be seen in Fig. 1, where in this case, x_1 , as an outgoing message from v_1 , is a function of the extrinsic state variables that are incoming messages to the missatisfied check nodes connected to v_1 . As another example, from Fig. 1, the channel LLR of the VN v_1 contributes to messages x_1 , x_2 and x_3 . This, based on (10), means that the elements in the first column of \mathbf{B} and rows 1, 2 and 3 are equal to 1. As the final example, the ones in the first column of \mathbf{B}_{ex} , which are located in rows 7 and 8, imply that the first unsatisfied CN message contributes to state variables x_7 and x_8 . This can also be seen from Fig. 1.

B. Application of Density Evolution in the State-Space Model

In order to analyze TS failures based on the linear state-space model, one needs to obtain the probability distribution of the messages entering the TS subgraph via unsatisfied CNs at different iterations, $\mathbf{L}_{ex}^{(\ell)}$, as well as the distribution of the messages from the external VNs connected to the missatisfied CNs. The latter distribution is then used to obtain the linear gains \bar{g}'_ℓ .

To obtain such distributions, the authors of [34], [42], [45] use density evolution (DE) [52] with the underlying assumptions that the all-zero codeword is transmitted, and that the surrounding neighborhood of the TS is tree-like. This implies that all the messages entering the TS through unsatisfied and missatisfied CNs are independent in each iteration as well as in subsequent iterations.

C. Missatisfied CN Gain Model

To calculate the missatisfied CN gains, without loss of generality, consider the missatisfied CN c_j in Fig. 1. The message passed from c_j to v_4 is given by

$$L_\ell^{[4 \leftarrow j]} = 2 \tanh^{-1} \left[g_\ell^{[j]} \tanh \frac{L_\ell^{[1 \rightarrow j]}}{2} \right], \quad (12)$$

where $g_\ell^{[j]}$ is defined as

$$g_\ell^{[j]} = \prod_{k \in N(j) \setminus \{1,4\}} \tanh \frac{L_\ell^{[k \rightarrow j]}}{2}. \quad (13)$$

For relatively small values of $L_\ell^{[1 \rightarrow j]}$ compared to $g_\ell^{[j]}$, which typically happens in the event of a TS failure, the Taylor expansion of order two for (12) around zero is given by

$$L_\ell^{[4 \leftarrow j]} \approx g_\ell^{[j]} L_\ell^{[1 \rightarrow j]}. \quad (14)$$

(Note that the square term in the Taylor expansion is equal to zero.) The above model is further simplified in [42], [45] by replacing $g_\ell^{[j]}$ with an average gain, \bar{g}_ℓ , over all possible channel noise realizations as well as all the CNs. For an LDPC code with regular CN degree of d_c , the expected gain is

$$\bar{g}_\ell = \mathbb{E}_{\mathbf{n},j,k} \left[\tanh \frac{L_\ell^{[k \rightarrow j]}}{2} \right]^{d_c-2}, \quad (15)$$

where \mathbf{n} is the channel noise vector. The average, $\mathbb{E}_{\mathbf{n},j,k}$, is taken over all CNs j , all $k \in N(j)$ and all noise realizations. To calculate (15), one can simply calculate the expected value with respect to the probability distribution of VN to CN messages at iteration ℓ , where this distribution is a function of degree distributions of the code as well as the channel noise distribution.

In [42], [45], the gain model of Equation (15) is extended by incorporating the polarity inversions of the LETS internal messages to the model. These inversions are caused by erroneous LLRs entering the missatisfied CNs from the $d_c - 2$ external VNs. In other words, assuming the all-zero codeword is transmitted, whenever an odd number of external messages, out of

$d_c - 2$, have negative signs, the polarity of the internal messages from missatisfied CNs to their neighboring VNs will be inverted. The probability of inversion, $P_{inv,\ell}$, is thus calculated by

$$P_{inv,\ell} = \sum_{k \text{ odd}} \binom{d_c - 2}{k} P_{e,\ell}^k (1 - P_{e,\ell})^{d_c - 2 - k}, \quad (16)$$

where $P_{e,\ell}$ is the probability of error in each of the VN to CN messages at iteration ℓ , and is calculated using DE. In [45], to model the inversion, the authors suggested using the following average gain instead of (15):

$$\bar{g}'_\ell = (1 - P_{inv,\ell})\bar{g}_\ell. \quad (17)$$

D. Error Probability of a LETS Structure

Before the calculation of error probability, we discuss some of the properties of the transition matrix \mathbf{A} relevant to the calculation.

For a given square matrix \mathbf{M} and a permutation matrix \mathbf{P} , the matrix \mathbf{PMP}^T is called the *symmetric permutation* of \mathbf{M} . If \mathbf{M} represents the adjacency matrix of a graph, symmetric permutation results in an isomorphic graph whose nodes are relabeled. The eigenvalues of \mathbf{M} and its symmetric permutation are the same. Also, their eigenvectors, up to a permutation, are equal [72].

Definition 1. A non-negative $n \times n$ real matrix \mathbf{M} is *irreducible* if it cannot be symmetrically permuted by any permutation matrix \mathbf{P} into a block upper triangular matrix, i.e.,

$$\mathbf{PMP}^T \neq \left[\begin{array}{c|c} \mathbf{M}_a & \mathbf{M}_c \\ \hline \mathbf{0} & \mathbf{M}_b \end{array} \right], \quad (18)$$

where \mathbf{M}_a and \mathbf{M}_b are square matrices with sizes greater than 0 (non-trivial). The matrix \mathbf{M} is *reducible* if it is not irreducible.

The *spectral radius* of a square matrix \mathbf{M} is defined as the largest absolute value of its eigenvalues, and is denoted by $\rho(\mathbf{M})$.

Theorem 1 (Perron-Frobenius theorem of non-negative irreducible matrices). *Let \mathbf{M} be a non-negative irreducible matrix. Then,*

- (a) \mathbf{M} has a positive real eigenvalue equal to its spectral radius $\rho(\mathbf{M})$.
- (b) corresponding to $\rho(\mathbf{M})$, matrix \mathbf{M} has a positive eigenvector \mathbf{x} .²

²This is valid for both left and right eigenvectors.

- (c) $\rho(\mathbf{M})$ is a simple (multiplicity equal to 1) eigenvalue of \mathbf{M} .
- (d) \mathbf{x} is the only non-negative eigenvector of \mathbf{M} .

Almost all the LETS structures, with the exception of simple cycles, have a non-negative irreducible transition matrix \mathbf{A} [45]. Hence, based on Theorem 1, there exists a positive dominant eigenvalue of \mathbf{A} , r , whose corresponding left and right eigenvectors, \mathbf{w}_1^T and \mathbf{u}_1 , are both positive. It is shown in [45] that for a simple cycle, $r = 1$, and for LETSs that are not simple cycles, $r > 1$.

To obtain the probability of a LETS failure, in [45], the authors first derived a non-recursive equation for the state vector:

$$\mathbf{x}^{(\ell)} = \mathbf{A}^\ell \mathbf{B} \mathbf{L} \prod_{j=1}^{\ell} \bar{g}'_j + \sum_{i=1}^{\ell} \mathbf{A}^{\ell-i} (\mathbf{B} \mathbf{L} + \mathbf{B}_{ex} \mathbf{L}_{ex}^{(i)}) \prod_{j=i+1}^{\ell} \bar{g}'_j. \quad (19)$$

They then showed that the projection of the state vector on the positive left eigenvector associated with the dominant eigenvalue r , given by

$$\mathbf{w}_1^T \mathbf{x}^{(\ell)} = r^\ell \mathbf{w}_1^T \mathbf{B} \mathbf{L} \prod_{j=1}^{\ell} \bar{g}'_j + \sum_{i=1}^{\ell} r^{\ell-i} \mathbf{w}_1^T (\mathbf{B} \mathbf{L} + \mathbf{B}_{ex} \mathbf{L}_{ex}^{(i)}) \prod_{j=i+1}^{\ell} \bar{g}'_j, \quad (20)$$

can be used as an indicator of TS failure. In fact, the following scaled version of (20) is used in [45] as the error indicator function:

$$\beta'_\ell = \mathbf{w}_1^T \mathbf{B} \mathbf{L} + \sum_{i=1}^{\ell} \frac{\mathbf{w}_1^T (\mathbf{B} \mathbf{L} + \mathbf{B}_{ex} \mathbf{L}_{ex}^{(i)})}{r^i \prod_{j=1}^i \bar{g}'_j}, \quad (21)$$

with the probability of error for the corresponding LETS \mathcal{S} given by

$$P_e(\mathcal{S}) = \lim_{\ell \rightarrow \infty} \Pr\{\beta'_\ell < 0\} = \lim_{\ell \rightarrow \infty} Q\left(\frac{\mathbb{E}[\beta'_\ell]}{\sqrt{\text{VAR}[\beta'_\ell]}}\right), \quad (22)$$

where $Q(x) = \frac{1}{\sqrt{2\pi}} \int_x^\infty \exp\left(-\frac{u^2}{2}\right) du$. In the derivation of (22), it is assumed that the random variable β'_ℓ is Gaussian.

IV. LINEAR STATE-SPACE MODEL OF LETSs FOR SPA WITH ROW LAYERED SCHEDULE

In this section, we develop a linear state-space model of LETSs for SPA with row layered schedule, and use the model to calculate the error probability of LETSs. In Subsection IV-A, by a proper labeling of state variables, we establish a relationship between the matrices \mathbf{A} , \mathbf{B} and \mathbf{B}_{ex} of the model for flooding schedule in (9)-(11) and the corresponding matrices needed in the model for the layered schedule. The recursive and non-recursive equations for the state vector

of the layered schedule are then derived in Subsection IV-B. In Subsection IV-C, we present the application of DE within the linear state-space model of the layered decoder. Within this subsection, we also introduce the concept of TS layer profile which plays an important role in the proper application of DE in the model, and in identifying TSs that have the same topology but may have different harmfulness. We then derive the gain values of the missatisfied CNs for a layered schedule in Subsection IV-D. The spectral properties of the LETS system matrices in layered decoders are analyzed in Subsection IV-E.

A. Relationship between model matrices of flooding and row layered schedules

To establish a relationship between the matrices that appear in the two models, it is helpful to label the state variables in a certain order. Consider an (a, b) LETS \mathcal{S} with m_s state variables x_1, \dots, x_{m_s} . Suppose that the missatisfied CNs of \mathcal{S} are from J different layers of the parity-check matrix \mathbf{H} , where $J \leq m_b$. We denote these layers by L_1, \dots, L_J , where an smaller index for a layer implies that the CNs in that layer are updated earlier in an iteration. In the following, we say that such a LETS has J layers. We use the notation n_{L_j} to denote the number of state variables that are updated in layer L_j , for $1 \leq j \leq J$. We thus have $n_{L_1} + \dots + n_{L_J} = m_s$. To assign the state variables to different internal messages of \mathcal{S} , we start with the messages that are updated in L_1 , and assign to them variables $x_1, \dots, x_{n_{L_1}}$. We then move on to the messages that are updated in L_2 , and assign to them variables $x_{n_{L_1}+1}, \dots, x_{n_{L_1}+n_{L_2}}$. We will continue this process all the way to L_J until all the m_s messages have their state variables assigned to them. We call this labeling of state variables *systematic labeling*.

Based on the systematic labeling, the matrix \mathbf{A} of flooding schedule will be a $J \times J$ array of matrices $\mathbf{A}_{i,j}$, $1 \leq i \leq J, 1 \leq j \leq J$, where the size of the matrix $\mathbf{A}_{i,j}$ is $n_{L_i} \times n_{L_j}$, and the J diagonal matrices are all-zero, i.e., $\mathbf{A}_{i,i} = \mathbf{0}, 1 \leq i \leq J$. Based on the partitioning of the state variables according to their layer, the rows of matrices \mathbf{B} and \mathbf{B}_{ex} can also be partitioned into J blocks, with the i th row block containing n_{L_i} rows. We refer to this representation of matrices as *systematic form*.

Example 2. Consider the $(5, 3)$ LETSs of the Tanner $(155, 64)$ code discussed in Example 1. The Tanner code has three row layers, i.e., $m_b = 3$. Each of the $(5, 3)$ LETSs has 3 unsatisfied and 6 missatisfied check nodes. Each of the three unsatisfied check nodes belongs to a different row layer. Out of 6 missatisfied check nodes, each set of two belongs to a different row layer ($J = 3$).

This is shown in Fig. 2. To distinguish the layers, different colors and line types are used in Fig. 2. As can be seen, the selection of edge labels, which reflects the indices of corresponding state variables, are in systematic form. The corresponding matrices are given by:

$$\mathbf{A} = \left[\begin{array}{c|c|c} \mathbf{0} & \mathbf{A}_{1,2} & \mathbf{A}_{1,3} \\ \hline \mathbf{A}_{2,1} & \mathbf{0} & \mathbf{A}_{2,3} \\ \hline \mathbf{A}_{3,1} & \mathbf{A}_{3,2} & \mathbf{0} \end{array} \right] = \left[\begin{array}{ccc|ccc|ccc} 0 & 0 & 0 & 0 & 0 & 0 & 0 & 1 & 0 & 1 & 0 & 0 \\ 0 & 0 & 0 & 0 & 0 & 0 & 0 & 0 & 0 & 0 & 0 & 1 \\ 0 & 0 & 0 & 0 & 0 & 0 & 1 & 0 & 0 & 0 & 0 & 0 \\ 0 & 0 & 0 & 0 & 1 & 0 & 0 & 0 & 0 & 0 & 0 & 1 \\ \hline 0 & 0 & 0 & 0 & 0 & 0 & 0 & 0 & 0 & 1 & 0 & 0 \\ 0 & 0 & 1 & 0 & 0 & 0 & 0 & 0 & 0 & 0 & 0 & 1 \\ 0 & 1 & 0 & 0 & 0 & 0 & 0 & 0 & 0 & 0 & 1 & 0 \\ 0 & 0 & 0 & 1 & 0 & 0 & 0 & 0 & 0 & 0 & 0 & 0 \\ \hline 0 & 1 & 0 & 0 & 0 & 0 & 0 & 0 & 1 & 0 & 0 & 0 \\ 0 & 0 & 0 & 0 & 0 & 1 & 0 & 0 & 0 & 0 & 0 & 0 \\ 1 & 0 & 0 & 0 & 0 & 0 & 0 & 0 & 0 & 0 & 0 & 0 \\ 0 & 0 & 1 & 0 & 1 & 0 & 0 & 0 & 0 & 0 & 0 & 0 \end{array} \right],$$

$$\mathbf{B} = \left[\begin{array}{c} \mathbf{B}_1 \\ \mathbf{B}_2 \\ \mathbf{B}_3 \end{array} \right] = \left[\begin{array}{cccc|cccc|cccc} 1 & 0 & 0 & 0 & 0 & 0 & 0 & 0 & 0 & 0 & 0 & 0 \\ 0 & 0 & 0 & 0 & 1 & 0 & 0 & 0 & 0 & 0 & 0 & 0 \\ 0 & 0 & 0 & 0 & 0 & 0 & 1 & 0 & 0 & 0 & 0 & 0 \\ 0 & 1 & 0 & 0 & 0 & 0 & 0 & 0 & 0 & 0 & 0 & 0 \\ \hline 0 & 0 & 1 & 0 & 0 & 0 & 0 & 0 & 0 & 0 & 0 & 0 \\ 0 & 1 & 0 & 0 & 0 & 0 & 0 & 0 & 0 & 0 & 0 & 0 \\ 1 & 0 & 0 & 0 & 0 & 0 & 0 & 0 & 0 & 0 & 0 & 0 \\ 0 & 0 & 0 & 0 & 0 & 0 & 1 & 0 & 0 & 0 & 0 & 0 \\ \hline 1 & 0 & 0 & 0 & 0 & 0 & 0 & 0 & 0 & 0 & 0 & 0 \\ 0 & 0 & 1 & 0 & 0 & 0 & 0 & 0 & 0 & 0 & 0 & 0 \\ 0 & 0 & 0 & 1 & 0 & 0 & 0 & 0 & 0 & 0 & 0 & 0 \\ 0 & 1 & 0 & 0 & 0 & 0 & 0 & 0 & 0 & 0 & 0 & 0 \end{array} \right], \mathbf{B}_{ex} = \left[\begin{array}{c} \mathbf{B}_{ex,1} \\ \mathbf{B}_{ex,2} \\ \mathbf{B}_{ex,3} \end{array} \right] = \left[\begin{array}{ccc|ccc|ccc} 0 & 0 & 0 & 0 & 0 & 0 & 0 & 0 & 0 & 0 & 0 & 0 \\ 0 & 1 & 0 & 0 & 0 & 0 & 0 & 0 & 0 & 0 & 0 & 0 \\ 0 & 0 & 1 & 0 & 0 & 0 & 0 & 0 & 0 & 0 & 0 & 0 \\ 0 & 0 & 0 & 0 & 0 & 0 & 0 & 0 & 0 & 0 & 0 & 0 \\ \hline 1 & 0 & 0 & 0 & 0 & 0 & 0 & 0 & 0 & 0 & 0 & 0 \\ 0 & 0 & 0 & 0 & 0 & 0 & 0 & 0 & 0 & 0 & 0 & 0 \\ 0 & 0 & 0 & 0 & 0 & 0 & 0 & 0 & 0 & 0 & 0 & 0 \\ 0 & 0 & 1 & 0 & 0 & 0 & 0 & 0 & 0 & 0 & 0 & 0 \\ \hline 0 & 0 & 0 & 0 & 0 & 0 & 0 & 0 & 0 & 0 & 0 & 0 \\ 1 & 0 & 0 & 0 & 0 & 0 & 0 & 0 & 0 & 0 & 0 & 0 \\ 0 & 1 & 0 & 0 & 0 & 0 & 0 & 0 & 0 & 0 & 0 & 0 \\ 0 & 0 & 0 & 0 & 0 & 0 & 0 & 0 & 0 & 0 & 0 & 0 \end{array} \right].$$

In a layered schedule, the state variables of a LETS are updated in J rounds, each round corresponding to one row layer, within one iteration. Corresponding to the updating of each layer, there thus exists a set of matrices used in the model. The $m_s \times m_s$ matrix that represents the relationship among the state variables corresponding to the updating of layer j is denoted by \mathcal{A}_j , $1 \leq j \leq J$, and is referred to as the “transition matrix of layer j .” Matrix \mathcal{A}_j has the same block structure as matrix \mathbf{A} . In fact, the j th row block of the two matrices are identical.

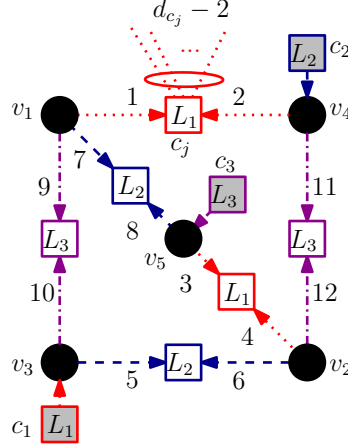


Fig. 2. A $(5, 3)$ LETS of the Tanner $(155, 64)$ code whose edges are labeled in a systematic form. The edges of different layers are distinguished by different colors and line types.

Matrix \mathcal{A}_j , however, has zero blocks everywhere else other than the diagonal blocks that are each an identity matrix. This is to indicate that as the messages in the j th layer are updated, all the other messages in the LETS remain unchanged. Similarly, notation \mathcal{B}_j is used to denote the $m_s \times a$ matrix that is responsible for the contribution of channel LLRs in the state variables that are updated in layer j . This matrix has the same row block structure as in \mathbf{B} , with the difference that except for row block j (consisting of n_{L_j} rows) that is identical to that of \mathbf{B} , all the other row blocks are zero. Similarly, for the contribution of unsatisfied CN messages to the state variables of layer j , the $m_s \times b$ matrix $\mathcal{B}_{ex,j}$ can be defined as a matrix with J row blocks whose j th row block is equal to that of B_{ex} while the other row blocks are all zero. This matrix, however, is not directly utilized in the model. The reason is that, two groups of unsatisfied CN messages contribute to the state variables in layer j at iteration ℓ . The first group are those that are updated at the end of $(\ell - 1)$ th iteration, $\mathbf{L}_{ex}^{(\ell-1)}$. The second group are the ones that are updated earlier in iteration ℓ , $\mathbf{L}_{ex}^{(\ell)}$. Correspondingly, the matrices $\overset{\triangleleft}{\mathcal{B}}_{ex,j}$ and $\overset{\triangleright}{\mathcal{B}}_{ex,j}$ are defined to account for the two contributions, respectively, and we have

$$\overset{\triangleleft}{\mathcal{B}}_{ex,j} + \overset{\triangleright}{\mathcal{B}}_{ex,j} = \mathcal{B}_{ex,j}. \quad (23)$$

Example 3. For the same LETS structure discussed in Example 2, the model matrices corre-

sponding to the second layer of row layered schedule are the followings:

$$\mathcal{A}_2 = \begin{bmatrix} \mathbf{I} & \mathbf{0} & \mathbf{0} \\ \mathbf{A}_{2,1} & \mathbf{0} & \mathbf{A}_{2,3} \\ \mathbf{0} & \mathbf{0} & \mathbf{I} \end{bmatrix}, \mathcal{B}_2 = \begin{bmatrix} \mathbf{0} \\ \mathbf{B}_2 \\ \mathbf{0} \end{bmatrix}, \overset{\triangleleft}{\mathcal{B}}_{ex,2} = \begin{bmatrix} 0 & 0 & 0 \\ 0 & 0 & 0 \\ 0 & 0 & 0 \\ 0 & 0 & 0 \\ \hline 0 & 0 & 0 \\ 0 & 0 & 0 \\ 0 & 0 & 0 \\ 0 & 0 & 0 \\ 0 & 0 & 1 \\ \hline 0 & 0 & 0 \\ 0 & 0 & 0 \\ 0 & 0 & 0 \\ 0 & 0 & 0 \end{bmatrix}, \overset{\triangleright}{\mathcal{B}}_{ex,2} = \begin{bmatrix} 0 & 0 & 0 \\ 0 & 0 & 0 \\ 0 & 0 & 0 \\ 0 & 0 & 0 \\ \hline 1 & 0 & 0 \\ 0 & 0 & 0 \\ 0 & 0 & 0 \\ 0 & 0 & 0 \\ 0 & 0 & 0 \\ \hline 0 & 0 & 0 \\ 0 & 0 & 0 \\ 0 & 0 & 0 \\ 0 & 0 & 0 \end{bmatrix}.$$

In the second layer, the unsatisfied CNs c_1 and c_3 contribute to the values of state variables x_5 and x_8 , respectively. While the message from c_1 is updated at the L_1 layer (before L_2), the message from c_3 is updated only in L_3 (after L_2). So, the contribution from c_1 to x_5 is reflected through $\overset{\triangleright}{\mathcal{B}}_{ex,2}$ which uses a newly updated (at the current iteration) version of CN message, while the contribution from c_3 to x_8 is via $\overset{\triangleleft}{\mathcal{B}}_{ex,2}$ and uses the CN message updated at the end of the previous iteration.

The last set of matrices that we need in the linear state-space model of a row layered decoder are the gain matrices. In the flooding schedule, the impact of external connections of the missatisfied CNs on the internal messages of a LETS is modelled by an iteration dependent scalar gain, \bar{g}_ℓ' [45]. This, in fact, corresponds to a diagonal gain matrix with equal diagonal elements, i.e., $\bar{g}_\ell' \mathbf{I}_{m_s \times m_s}$, and assumes that all the missatisfied CNs have equal impact on the internal messages of the LETS. For a layered decoder, however, there can be a significant difference among the distribution of external messages of different missatisfied CNs, depending on their layer and their external connections. To model the missatisfied CN gains within a given layer j at iteration ℓ , we thus use the gain matrix $\mathcal{G}_j^{(\ell)}$. To define $\mathcal{G}_j^{(\ell)}$, we first consider the following $m_s \times m_s$ diagonal matrix:

$$\mathbf{G}^{(\ell)} = \begin{bmatrix} \bar{g}_1'^{(\ell)} & 0 & \cdots & 0 \\ 0 & \bar{g}_2'^{(\ell)} & \ddots & \vdots \\ \vdots & \ddots & \ddots & 0 \\ 0 & \cdots & 0 & \bar{g}_{m_s}'^{(\ell)} \end{bmatrix},$$

whose diagonal entries are the linear gains corresponding to m_s state variables. (Note that the state variables corresponding to the same missatisfied CN have equal gains.) We then partition $\mathbf{G}^{(\ell)}$ into $J \times J$ block matrices. This partitioning corresponds to different layers of the LETS and is similar to the partitioning of the transition matrix \mathbf{A} . As a result, we have

$$\mathbf{G}^{(\ell)} = \begin{bmatrix} \mathbf{G}_1^{(\ell)} & \mathbf{0} & \mathbf{0} & \cdots & \mathbf{0} \\ \mathbf{0} & \mathbf{G}_2^{(\ell)} & \mathbf{0} & \cdots & \mathbf{0} \\ \mathbf{0} & \mathbf{0} & \ddots & \ddots & \vdots \\ \vdots & \vdots & \ddots & \ddots & \mathbf{0} \\ \mathbf{0} & \mathbf{0} & \cdots & \mathbf{0} & \mathbf{G}_J^{(\ell)} \end{bmatrix}.$$

Now, the gain matrix $\mathcal{G}_j^{(\ell)}$ corresponding to layer j is defined as $\mathbf{G}^{(\ell)}$ in which all the diagonal blocks, except the j th one, are replaced with the identity matrix. For example, for $j = 2$,

$$\mathcal{G}_2^{(\ell)} = \begin{bmatrix} \mathbf{I} & \mathbf{0} & \mathbf{0} & \cdots & \mathbf{0} \\ \mathbf{0} & \mathbf{G}_2^{(\ell)} & \mathbf{0} & \cdots & \mathbf{0} \\ \mathbf{0} & \mathbf{0} & \mathbf{I} & \ddots & \vdots \\ \vdots & \vdots & \ddots & \ddots & \mathbf{0} \\ \mathbf{0} & \mathbf{0} & \cdots & \mathbf{0} & \mathbf{I} \end{bmatrix}.$$

B. Linear State-Space Model of LETSs for Row Layered SPA

Using the matrices presented in the previous subsection, we have the following linear state-space model of a LETS for row layered SPA:

$$\tilde{\mathbf{x}}^{(0,j)} = \mathbf{0} \quad \text{for } \ell = 0, 1 \leq j \leq J \quad (24)$$

$$\begin{aligned} \tilde{\mathbf{x}}^{(\ell,j)} = & \quad \text{for } \ell \geq 1, 1 \leq j \leq J \\ & \mathcal{G}_j^{(\ell)} (\mathcal{A}_j \tilde{\mathbf{x}}^{(\ell-\delta_{j1}, j-1+J\delta_{j1})} + \mathcal{B}_j \mathbf{L} + \overset{\triangleleft}{\mathcal{B}}_{ex,j} \mathbf{L}_{ex}^{(\ell-1)} + \overset{\triangleright}{\mathcal{B}}_{ex,j} \mathbf{L}_{ex}^{(\ell)}). \end{aligned} \quad (25)$$

In the above model, the state vector at layer j of iteration ℓ is denoted by $\tilde{\mathbf{x}}^{(\ell,j)}$. The vectors \mathbf{L} , $\mathbf{L}_{ex}^{(\ell-1)}$ and $\mathbf{L}_{ex}^{(\ell)}$ are the inputs to the model and represent channel LLRs and messages from unsatisfied CNs at iterations $\ell-1$ and ℓ , respectively, where $\mathbf{L}_{ex}^{(0)} = \mathbf{0}$. Also, δ_{j1} , is the Kronecker delta function which is equal to 1, when $j = 1$, and is zero, otherwise. Equation (25) implies that at the first layer of every iteration, the state vector is updated based on the state vector from

the last layer of the previous iteration, while in the other layers, the updated states are a function of the state vector of the previous layer within the same iteration.

Next, we use induction to derive a non-recursive equation for the state vector at the end of iteration ℓ , i.e., $\tilde{\mathbf{x}}^{(\ell,J)}$. For this, we first define some new matrices. The first matrix is defined as

$$\tilde{\mathbf{A}}_{J \rightarrow k}^{(\ell)} = (\mathcal{G}_J^{(\ell)} \mathcal{A}_J)(\mathcal{G}_{J-1}^{(\ell)} \mathcal{A}_{J-1}) \cdots (\mathcal{G}_k^{(\ell)} \mathcal{A}_k), \quad (26)$$

which is, an ordered multiplication of the scaled version of transition matrices of different layers, $\mathcal{G}_j^{(\ell)} \mathcal{A}_j$, from the layer with maximum index J down to the k th layer, $k \geq 1$. By using $\tilde{\mathbf{A}}_{J \rightarrow k}^{(\ell)}$, we define three other matrices as follows:

$$\tilde{\mathbf{B}}^{(\ell)} = \tilde{\mathbf{A}}_{J \rightarrow 2}^{(\ell)} \mathcal{G}_1^{(\ell)} \mathcal{B}_1 + \tilde{\mathbf{A}}_{J \rightarrow 3}^{(\ell)} \mathcal{G}_2^{(\ell)} \mathcal{B}_2 + \cdots + \mathcal{G}_J^{(\ell)} \mathcal{B}_J, \quad (27)$$

$$\overset{\triangleright}{\mathbf{B}}_{ex}^{(\ell)} = \tilde{\mathbf{A}}_{J \rightarrow 2}^{(\ell)} \mathcal{G}_1^{(\ell)} \overset{\triangleright}{\mathcal{B}}_{ex,1} + \tilde{\mathbf{A}}_{J \rightarrow 3}^{(\ell)} \mathcal{G}_2^{(\ell)} \overset{\triangleright}{\mathcal{B}}_{ex,2} + \cdots + \mathcal{G}_J^{(\ell)} \overset{\triangleright}{\mathcal{B}}_{ex,J}, \quad (28)$$

$$\overset{\triangleleft}{\mathbf{B}}_{ex}^{(\ell)} = \tilde{\mathbf{A}}_{J \rightarrow 2}^{(\ell)} \mathcal{G}_1^{(\ell)} \overset{\triangleleft}{\mathcal{B}}_{ex,1} + \tilde{\mathbf{A}}_{J \rightarrow 3}^{(\ell)} \mathcal{G}_2^{(\ell)} \overset{\triangleleft}{\mathcal{B}}_{ex,2} + \cdots + \mathcal{G}_J^{(\ell)} \overset{\triangleleft}{\mathcal{B}}_{ex,J}. \quad (29)$$

Finally, the non-recursive formula of the state vector at the end of iteration ℓ is derived as

$$\tilde{\mathbf{x}}^{(\ell,J)} = \sum_{i=1}^{\ell} \left(\overset{\rightarrow}{\prod}_{j=i+1}^{\ell} \tilde{\mathbf{A}}_{J \rightarrow 1}^{(j)} \right) \tilde{\mathbf{B}}^{(i)} \mathbf{L} + \sum_{i'=1}^{\ell} \left(\overset{\rightarrow}{\prod}_{j'=i'+1}^{\ell} \tilde{\mathbf{A}}_{J \rightarrow 1}^{(j')} \right) \left(\overset{\triangleleft}{\mathbf{B}}_{ex}^{(i')} \mathbf{L}_{ex}^{(i'-1)} + \overset{\triangleright}{\mathbf{B}}_{ex}^{(i')} \mathbf{L}_{ex}^{(i')} \right), \quad (30)$$

where the right arrow on top of the product sign denotes the matrix product applied from the left. For example,

$$\overset{\rightarrow}{\prod}_{j=i+1}^{\ell} \tilde{\mathbf{A}}_{J \rightarrow 1}^{(j)} = \tilde{\mathbf{A}}_{J \rightarrow 1}^{(\ell)} \tilde{\mathbf{A}}_{J \rightarrow 1}^{(\ell-1)} \cdots \tilde{\mathbf{A}}_{J \rightarrow 1}^{(i+1)}.$$

In the rest of the paper, since we only consider the state vector $\tilde{\mathbf{x}}^{(\ell,J)}$ at the end of each iteration, for simplicity, we may drop the index J , and represent the state vector by $\tilde{\mathbf{x}}^{(\ell)}$.

In Subsection V-A, Equation (30) will be used to estimate the probability of a LETS failure in the layered decoder.

C. The Application of DE to the Layered Decoder

In the state-space analysis of layered decoders, we use DE to calculate the distribution of messages entering the LETS from the rest of the Tanner graph. To apply DE to a layered decoder of a QC-LDPC code, for each iteration, one needs to derive two distributions corresponding to each edge e of the base graph. The two distributions correspond to the messages passed from CNs

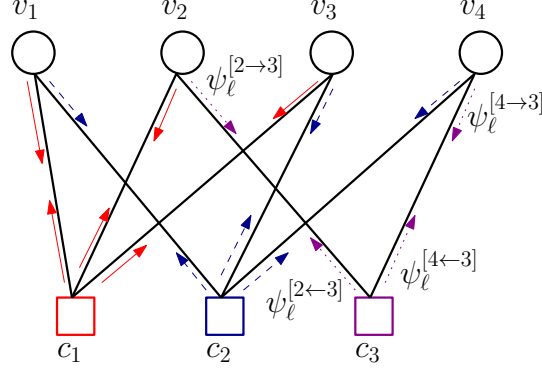


Fig. 3. Base graph of Example 4: The solid (red), dashed (blue) and dotted (purple) arrows, correspond to messages passed within layers L_1 to L_3 , respectively. The symbols next to the dotted arrows show the probability distributions of messages updated in the 3rd layer of the ℓ th iteration.

(VNs) to VNs (CNs) of the Tanner graph that are connected by the cluster of edges associated with e . If edge e connects VN i to CN j in the base graph, we say that the cluster of edges corresponding to e connect Type- i VNs to Type- j CNs in the Tanner graph. The computation tree for the calculation of such distributions is not only a function of the base graph but also depends on the order in which the messages of different row layers are updated. To identify these distributions, we use the notations $\psi_\ell^{[i \rightarrow j]}$ and $\psi_\ell^{[i \leftarrow j]}$ to denote the probability distribution of the messages from Type- i VNs to Type- j CNs and vice versa in iteration ℓ , respectively.

Example 4. Consider the base graph of Fig. 3 corresponding to the following base matrix:

$$\mathbf{H}_b = \begin{bmatrix} 1 & 1 & 1 & 0 \\ 1 & 0 & 1 & 1 \\ 0 & 1 & 0 & 1 \end{bmatrix}. \quad (31)$$

The messages updated in different layers are identified on the base graph with different colors and line types. Suppose that the three layers are updated in accordance to the increasing row index. The computation trees of some of the CN to VN messages for the first iteration are demonstrated in Figs. 4a to 4d. As can be seen, the computation trees are different depending on the type of the VN at the root, and the type of the connecting CN. In particular, the trees have different depths within the same iteration. The trees will also change by changing the order in which the layers are updated. This is unlike the flooding schedule, for which the depth of all computation trees at iteration ℓ is 2ℓ regardless of the type of VNs or CNs, or any permutation

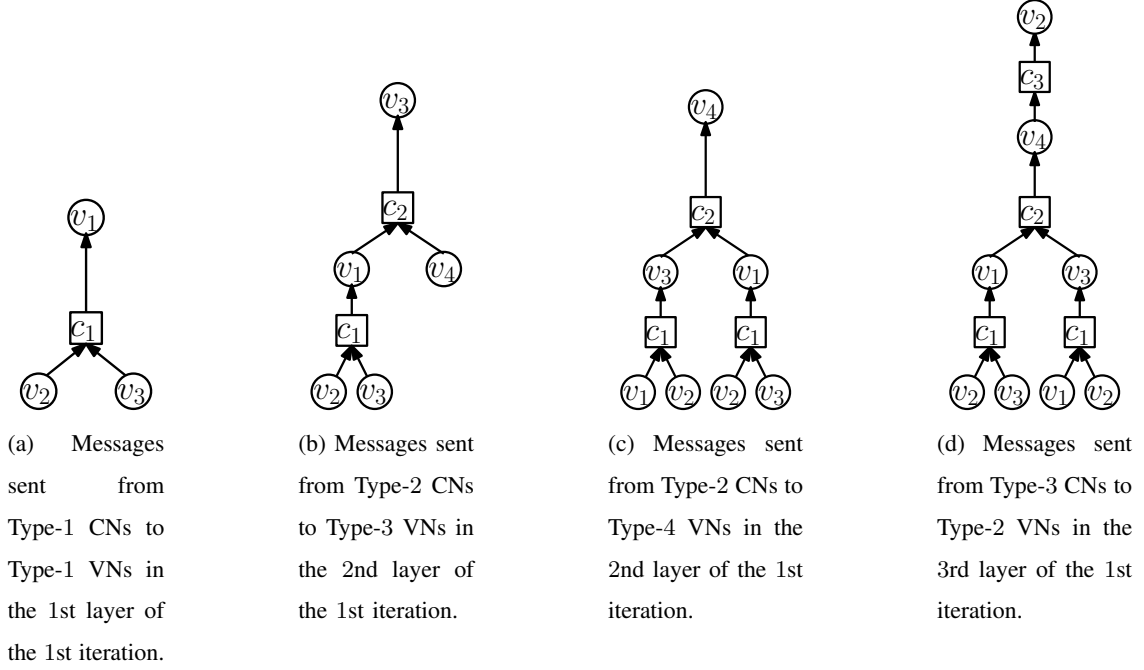


Fig. 4. The computation trees of certain messages at different layers of the 1st iteration.

of row layers. This implies that, for a layered decoder, the message distributions change with changing the order in which the row layers are updated.

Consider a LETS whose missatisfied CNs belong to J layers, L_1, \dots, L_J . Consider a permutation π over the set of integer numbers $\{1, \dots, J\}$. Assume that the messages within the row layers of the parity-check matrix (within one iteration) are updated such that CNs with type $\pi(1)$ within the LETS are updated first, followed by CNs with type $\pi(2)$ and so on. This means that missatisfied CNs of the LETS that belong to L_i are of Type- $\pi(i)$, for $i = 1, \dots, J$. To obtain the distribution of incoming messages to the LETS from the rest of the Tanner graph using DE, one needs to know not only the topology of the TS, but also the following information:

- 1) types of all missatisfied and unsatisfied CNs of the TS as well as the layer to which each CN of the TS belongs (the latter corresponds to knowing the permutation π),
- 2) the type and layer of all the variable nodes that are externally connected to all the missatisfied CNs, and the type and layer of all internal VNs connected to unsatisfied CNs.

We refer to the above information as *TS layer profile* (TSLP). We note that the TSLP can be different for isomorphic TSs, thus, resulting in different harmfulness for such TSs.

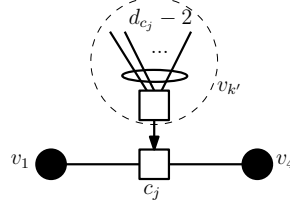


Fig. 5. The external messages of a missatisfied CN are represented by a virtual VN.

Example 5. Consider the $(5, 3)$ LETS of Fig. 2, and assume that the layers of the code are updated in the increasing order of row indices. Variable nodes v_1 and v_5 are of Type-3 and Type-5, respectively, while VNs v_2 , v_3 and v_4 , are of Type-1. As an example of a missatisfied CN, consider c_j . Check node c_j is of Type-1 and is in L_1 . Also, the $d_{c_j} - 2 = 3$ external VNs of c_j are of Type-2, -4 and -5, respectively. As a result, to derive the gain value corresponding to c_j in the linear state-space model, one needs the probability distributions of messages from Type-2, -4 and -5 VNs sent to Type-1 CNs from the DE results. As an example of an unsatisfied CN, consider c_2 . Check node c_2 is of Type-2 and is in L_2 , and is connected to the internal VN v_4 , which is of Type-1. The probability distribution of the messages sent from c_2 to v_4 , thus follows the DE results for messages from Type-2 CNs to Type-1 VNs.

The following lemma follows directly from the fact that a QC-LDPC code is a cyclic lifting of the corresponding base code.

Lemma 1. Let p be the lifting degree of a QC-LDPC code \mathcal{C} , and let \mathcal{S} be a LETS of \mathcal{C} . Then, the TSLP of \mathcal{S} is the same as the TSLP of any of the isomorphic LETSs whose VNs are obtained by circularly shifting (modulo p) the VNs of \mathcal{S} .

D. Missatisfied CN Gain Model in Layered Decoders

In Subsection IV-A, we introduced the matrix $\mathbf{G}^{(\ell)}$ whose diagonal elements are the gains associated with missatisfied CNs at different layers of the ℓ th iteration. Due to the difference in the distributions of external messages entering different missatisfied CNs, the gain for each missatisfied CN needs to be calculated separately. For simplicity, the external connections of each missatisfied CN are represented by a virtual VN, as shown in Fig. 5. Without loss of generality, we consider VNs v_1 and v_4 of the $(5, 3)$ LETS of Fig. 2 with the missatisfied CN c_j connecting them (as shown in Fig. 5). The virtual VN is denoted by $v_{k'}$ in Fig. 5. The message

$L_\ell^{[4 \leftarrow j]}$ can then be calculated as

$$L_\ell^{[4 \leftarrow j]} = f(L_\ell^{[1 \rightarrow j]}, L_\ell^{[k' \rightarrow j]}), \quad (32)$$

where $f(\cdot, \cdot)$ is the box-plus operation given in (7). For small values of $L_\ell^{[1 \rightarrow j]}$, i.e., $L_\ell^{[1 \rightarrow j]} \approx 0$, the CN linear estimation based on Taylor expansion can be obtained as

$$L_\ell^{[4 \leftarrow j]} \approx f_{x_1}(0, L_\ell^{[k' \rightarrow j]}) L_\ell^{[1 \rightarrow j]}, \quad (33)$$

where f_{x_1} represents the partial derivative of $f(x_1, x_2)$ with respect to x_1 . We thus have

$$\begin{aligned} f_{x_1}(0, L_\ell^{[k' \rightarrow j]}) &= \ln \left(\frac{e^{L_\ell^{[k' \rightarrow j]}} - 1}{e^{L_\ell^{[k' \rightarrow j]}} + 1} \right) \\ &= \tanh \left(\frac{L_\ell^{[k' \rightarrow j]}}{2} \right). \end{aligned} \quad (34)$$

The average gain corresponding to CN c_j , $\bar{g}_{c_j}^{(\ell)}$, is then obtained as

$$\bar{g}_{c_j}^{(\ell)} = \int_{-\infty}^{\infty} \tanh\left(\frac{\lambda}{2}\right) \hat{\psi}_\ell^{[k' \rightarrow j]}(\lambda) d\lambda, \quad (35)$$

in which $\hat{\psi}_\ell^{[k' \rightarrow j]}$ is the probability distribution of the message from virtual VN, $v_{k'}$, to the missatisfied CN c_j at iteration ℓ . Given the TSLP of a LETS, this distribution can be calculated for different missatisfied CNs using DE. It is noted that there are $\frac{m_s}{2}$ missatisfied CNs in a LETS subgraph, and that each of the gains calculated by (35) should be used for the two state variables that have the corresponding CN in common.

We further modify Equation (35) to take into account the effect of polarity inversion, i.e., whenever an error occurs in the messages from the virtual VN, $v_{k'}$, for $k' = \{1, \dots, \frac{m_s}{2}\}$, the polarity of the state variables passing through the corresponding missatisfied CN is altered. The probability of polarity inversion is thus calculated by

$$P_{inv, \ell}^{[k' \rightarrow j]} = \int_{-\infty}^0 \hat{\psi}_\ell^{[k' \rightarrow j]}(\lambda) d\lambda. \quad (36)$$

To incorporate the polarity inversion in the model, we modify the average gains as follows:

$$\bar{g}_{c_j}'^{(\ell)} = (1 - P_{inv, \ell}^{[k' \rightarrow j]}) \bar{g}_{c_j}^{(\ell)}, \quad (37)$$

where $\bar{g}_{c_j}^{(\ell)}$ is given by (35).

E. Spectral Properties of LETS System Matrices in Layered Decoders

A careful study of Equation (30) reveals that the iteration dependent matrix

$$\tilde{\mathbf{A}}_{J \rightarrow 1}^{(\ell)} = (\mathcal{G}_J^{(\ell)} \mathcal{A}_J)(\mathcal{G}_{J-1}^{(\ell)} \mathcal{A}_{J-1}) \dots (\mathcal{G}_1^{(\ell)} \mathcal{A}_1), \quad (38)$$

plays a crucial role in the evolution of the state vector, and consequently in the failure rate, of a LETS. In the event of a failure, as the iterations progress, the average gains of missatisfied CNs tend to one. We thus have

$$\lim_{\ell \rightarrow \infty} \tilde{\mathbf{A}}_{J \rightarrow 1}^{(\ell)} = \mathcal{A}_J \mathcal{A}_{J-1} \dots \mathcal{A}_1 \triangleq \tilde{\mathbf{A}}_{J \rightarrow 1}. \quad (39)$$

The matrix $\tilde{\mathbf{A}}_{J \rightarrow 1}$, obtained by the multiplication of transition matrices of different layers of the LETS, is iteration independent. In the state-space analysis of the layered decoder, $\tilde{\mathbf{A}}_{J \rightarrow 1}$ plays a similar role as the transition matrix \mathbf{A} does in the model for a flooding decoder. In the following, we refer to $\tilde{\mathbf{A}}_{J \rightarrow 1}$ as the transition matrix of the layered decoder, and investigate its spectral properties. In particular, we demonstrate that, unlike the case for flooding where for majority of LETSs, the transition matrix \mathbf{A} is irreducible, the transition matrix $\tilde{\mathbf{A}}_{J \rightarrow 1}$ for layered decoding is reducible. We also show that the spectral radius of $\tilde{\mathbf{A}}_{J \rightarrow 1}$ is always larger than that of \mathbf{A} .

Using the systematic form of system model matrices as described in Subsection IV-A, the first column block of the transition matrix $\tilde{\mathbf{A}}_{J \rightarrow 1}$, consisting of n_{L_1} columns, is zero. We thus have the following result.

Lemma 2. *The transition matrix $\tilde{\mathbf{A}}_{J \rightarrow 1}$ of a LETS in a layered decoder is reducible.*

Example 6. *The transition matrix, $\tilde{\mathbf{A}}_{3 \rightarrow 1}$, of the (5, 3) LETS in Fig. 2 (also considered in Examples 2 and 3) is equal to*

$$\begin{aligned}
\tilde{\mathbf{A}}_{3 \rightarrow 1} = \mathcal{A}_3 \mathcal{A}_2 \mathcal{A}_1 &= \left[\begin{array}{c|cc} \mathbf{0} & \mathbf{A}_{1,2} & \mathbf{A}_{1,3} \\ \hline \mathbf{0} & \mathbf{A}_{2,1} \mathbf{A}_{1,2} & \mathbf{A}_{2,1} \mathbf{A}_{1,3} + \mathbf{A}_{2,3} \\ \hline \mathbf{0} & \mathbf{A}_{3,1} \mathbf{A}_{1,2} + \mathbf{A}_{3,2} \mathbf{A}_{2,1} \mathbf{A}_{1,2} & \mathbf{A}_{3,1} \mathbf{A}_{1,3} + \mathbf{A}_{3,2} \mathbf{A}_{2,1} \mathbf{A}_{1,3} + \mathbf{A}_{3,2} \mathbf{A}_{2,3} \end{array} \right] \\
&= \left[\begin{array}{cccc|cccc|cccc} 0 & 0 & 0 & 0 & 0 & 0 & 0 & 1 & 0 & 1 & 0 & 0 \\ 0 & 0 & 0 & 0 & 0 & 0 & 0 & 0 & 0 & 0 & 0 & 1 \\ 0 & 0 & 0 & 0 & 0 & 0 & 1 & 0 & 0 & 0 & 0 & 0 \\ 0 & 0 & 0 & 0 & 1 & 0 & 0 & 0 & 0 & 0 & 1 & 0 \\ \hline 0 & 0 & 0 & 0 & 0 & 0 & 0 & 0 & 1 & 0 & 0 & 0 \\ 0 & 0 & 0 & 0 & 0 & 0 & 1 & 0 & 0 & 0 & 1 & 0 \\ 0 & 0 & 0 & 0 & 0 & 0 & 0 & 0 & 0 & 1 & 0 & 1 \\ 0 & 0 & 0 & 0 & 1 & 0 & 0 & 0 & 0 & 0 & 1 & 0 \\ \hline 0 & 0 & 0 & 0 & 1 & 0 & 0 & 0 & 0 & 0 & 1 & 1 \\ 0 & 0 & 0 & 0 & 0 & 0 & 1 & 0 & 0 & 0 & 1 & 0 \\ 0 & 0 & 0 & 0 & 0 & 0 & 0 & 1 & 0 & 1 & 0 & 0 \\ 0 & 0 & 0 & 0 & 0 & 0 & 1 & 0 & 1 & 0 & 0 & 0 \end{array} \right]. \tag{40}
\end{aligned}$$

Theorem 2. [73, p. 50] For every real $n \times n$ matrix \mathbf{M} , there exists an $n \times n$ permutation matrix \mathbf{P} such that

$$\mathbf{PMP}^T = \left[\begin{array}{cccc} \mathbf{M}_{1,1} & \mathbf{M}_{1,2} & \cdots & \mathbf{M}_{1,t} \\ 0 & \mathbf{M}_{2,2} & \cdots & \mathbf{M}_{2,t} \\ \vdots & \ddots & \ddots & \vdots \\ 0 & \cdots & 0 & \mathbf{M}_{t,t} \end{array} \right], \tag{41}$$

is a $t \times t$ array of matrices, where each of the diagonal matrices $\mathbf{M}_{i,i}$, $1 \leq i \leq t$, is either irreducible or a 1×1 null matrix (zero).

The form of a matrix given by (41) is called *Frobenius normal form* or FNF, in brief. In the above theorem, if \mathbf{M} is irreducible, then $t = 1$.

Theorem 3. [73, p. 51] Let \mathbf{M} be an $n \times n$ non-negative matrix. Then,

- (a) \mathbf{M} has a real non-negative eigenvalue equal to its spectral radius $\rho(\mathbf{M})$. In addition, the corresponding real eigenvalue is positive unless \mathbf{M} is reducible and its FNF is strictly upper

triangular.³

(b) *The associated eigenvector of $\rho(\mathbf{M})$ is non-negative.*

The proof of Theorem 3 follows from Theorem 1 if \mathbf{M} is irreducible. If \mathbf{M} is reducible, then by considering the FNF \mathbf{PMP}^T of \mathbf{M} , and the fact that the eigenvalues of \mathbf{M} are the union of the eigenvalues of the diagonal matrices of FNF, one can see that \mathbf{M} has either a real positive eigenvalue equal to its spectral radius (if there is at least one irreducible diagonal matrix in FNF), or the spectral radius is zero (if all the diagonal matrices of FNF are 1×1 zero matrices).

Theorem 4. [74, Theorem 22] *Let \mathbf{M} be an $n \times n$ real non-negative matrix. Suppose that for a non-negative vector $\mathbf{x} \geq \mathbf{0}$ and $\mathbf{x} \neq \mathbf{0}$, we have $\mathbf{Mx} - \beta\mathbf{x} \geq \mathbf{0}$, where $\beta > 0$ is a constant. Then,*

$$\rho(\mathbf{M}) \geq \beta,$$

with the inequality being strict if $\mathbf{Mx} - \beta\mathbf{x} > \mathbf{0}$.

The following result is simple to prove.

Lemma 3. *Let $\tilde{\mathbf{A}}_{J \rightarrow 1}$ and \mathbf{A} be the transition matrices of a LETS in layered and flooding decoders, respectively. We then have*

$$\tilde{\mathbf{A}}_{J \rightarrow 1} = \mathbf{A} + \mathbf{A}'(\mathbf{A} - \mathbf{I}), \quad (42)$$

where

$$\mathbf{A}' = \mathbf{A}_l^{J-1} + \mathbf{A}_l^{J-2} + \cdots + \mathbf{A}_l, \quad (43)$$

and \mathbf{A}_l is a lower triangular matrix whose non-zero elements (under main diagonal) are equal to those of matrix \mathbf{A} .

Proposition 1. *Let $\tilde{\mathbf{A}}_{J \rightarrow 1}$ and \mathbf{A} be the transition matrices of a LETS in layered and flooding decoders, respectively. If \mathbf{A} is irreducible, then*

$$\rho(\tilde{\mathbf{A}}_{J \rightarrow 1}) \geq \rho(\mathbf{A}).$$

³A matrix \mathbf{M} is called strictly upper triangular if $\mathbf{M}(i, j) = 0$ for $i \geq j$, where $\mathbf{M}(i, j)$ denotes the element of \mathbf{M} in the i th row and the j th column.

Proof. Since \mathbf{A} is irreducible, it has a simple positive eigenvalue, r , which is equal to $\rho(\mathbf{A})$. To r , there corresponds a positive right eigenvector, \mathbf{u}_1 . By right multiplication of (42) with \mathbf{u}_1 , we have

$$\tilde{\mathbf{A}}_{J \rightarrow 1} \mathbf{u}_1 = r \mathbf{u}_1 + \mathbf{A}'(r - 1) \mathbf{u}_1. \quad (44)$$

Since $r > 1$, $\mathbf{u}_1 > \mathbf{0}$ and $\mathbf{A}' \geq \mathbf{0}$, we have $\mathbf{A}'(r - 1) \mathbf{u}_1 \geq \mathbf{0}$ and $r \mathbf{u}_1 > \mathbf{0}$, and therefore

$$\tilde{\mathbf{A}}_{J \rightarrow 1} \mathbf{u}_1 - r \mathbf{u}_1 \geq \mathbf{0}. \quad (45)$$

Using this in Theorem 4 completes the proof. \blacksquare

Based on Lemma 2, we know that $\tilde{\mathbf{A}}_{J \rightarrow 1}$ is a non-negative reducible matrix. As a result, the FNF of $\tilde{\mathbf{A}}_{J \rightarrow 1}$ has either irreducible or 1×1 null matrices as its diagonal blocks. In the following, we demonstrate that the FNF of $\tilde{\mathbf{A}}_{J \rightarrow 1}$ has only one irreducible diagonal block with all the other blocks being equal to 1×1 zero matrices. To show this, we use the directed edge graph (digraph) representation of the transition matrices. This representation, which was also used in [45], represents each state variable with a node in the graph and the dependencies among them by directed edges, i.e., a directed edge $x_i x_j$ in the graph means that state variable x_j , corresponding to the *head* node of the edge, at iteration ℓ is a function of state variable x_i , corresponding to the *tail* node of the edge, at iteration $\ell - 1$. In the digraph, the tail (head) nodes of all the incoming (outgoing) edges of a node x , i.e., all the edges with head (tail) x , are called the *parents* (*children*) of x .

It appears that the adjacency matrix of the digraph is equal to the transpose of the transition matrix. In the following, we use notations $D_f(\mathcal{S}) = (V_f, E_f)$ and $D_l(\mathcal{S}) = (V_l, E_l)$ to denote the digraphs corresponding to a LETS \mathcal{S} in flooding and layered decoding, respectively, where the set of nodes and edges in each graph are denoted by V and E , respectively, with indices f and l indicating “flooding” and “layered,” respectively.

A digraph is *strongly connected* if there exists a directed walk between any pair of its nodes. Consider a LETS \mathcal{S} with an irreducible transition matrix \mathbf{A} in a flooding decoder. The irreducibility of \mathbf{A} implies that the digraph $D_f(\mathcal{S}) = (V_f, E_f)$ is strongly connected [75].

Example 7. The digraph $D_f(\mathcal{S})$ of the flooding decoder for the $(5, 3)$ LETS of Fig. 2 is shown in Fig. 6a. As can be seen this digraph is strongly connected.

The digraph $D_l(\mathcal{S})$ of a LETS \mathcal{S} for a layered decoder can be obtained from its adjacency matrix $\tilde{\mathbf{A}}_{J \rightarrow 1}^T$. The digraph $D_l(\mathcal{S})$ can also be constructed from the flooding digraph $D_f(\mathcal{S})$

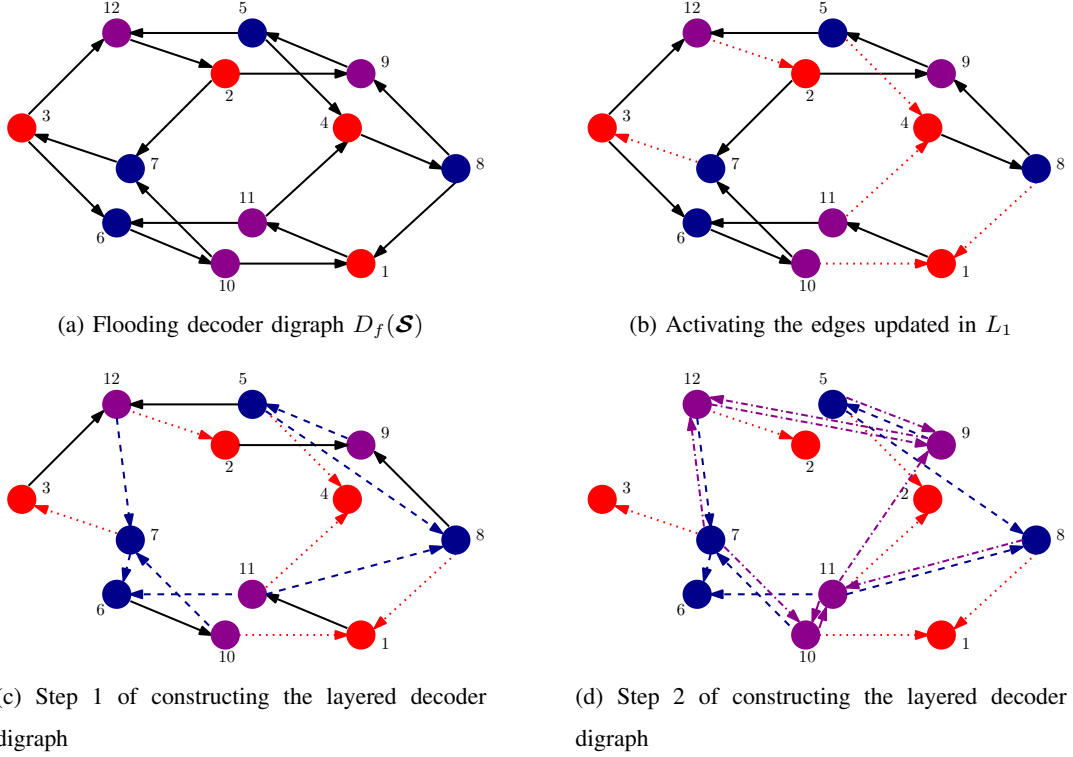


Fig. 6. The steps of constructing the digraph $D_l(\mathcal{S})$ of the $(5, 3)$ LETS for a layered decoder from the flooding digraph $D_f(\mathcal{S})$. (The colors (edge types) red (dotted), blue (dashed) and purple (dash-dotted) represent L_1 , L_2 and L_3 , respectively.)

through $J - 1$ steps, each corresponding to one layer of decoding. In step j , $j = 1, \dots, J - 1$, one considers all the nodes corresponding to state variables that are updated in layer L_{j+1} and their incoming edges. If the tail of any of such incoming edges has been updated in the previous layers within the same iteration, then the incoming edge is removed and new incoming edges are created from the parents of the updated tail to the head of the removed edge.

Example 8. The steps for the construction of $D_l(\mathcal{S})$ from $D_f(\mathcal{S})$ for the $(5, 3)$ LETS of Fig. 2 are shown in Fig. 6, where different colors and line types are used to identify the state variables and updated edges in different layers. It can be verified that the adjacency matrix of the resulted digraph of Fig. 6d is equal to the transpose of the matrix $\tilde{\mathbf{A}}_{3 \rightarrow 1}$, given in Equation (40). In particular, the zero columns of matrix $\tilde{\mathbf{A}}_{3 \rightarrow 1}$ correspond to nodes of Fig. 6d with no outgoing edges.

The following result follows from the construction of $D_l(\mathcal{S})$ from $D_f(\mathcal{S})$.

Lemma 4. Consider a state variable $v \in V_f$ of $D_f(\mathcal{S})$, for a LETS \mathcal{S} , updated in layer L_k ,

$k = \{1, 2, \dots, J\}$. If all the outgoing edges of v are connected to nodes from subsequent layers L_j , $k < j \leq J$, the corresponding node $v \in V_l$ of $D_l(\mathcal{S})$ will not have any outgoing edges. The total number of nodes n_z in $D_l(\mathcal{S})$ that have this property are greater than or equal to the number of nodes updated in the first layer, i.e., $n_z \geq n_{L_1}$.

The following lemma applies to LETSs with irreducible transition matrices \mathbf{A} for flooding schedule, and follows from the construction of $D_l(\mathcal{S})$ from $D_f(\mathcal{S})$ and the fact that for such LETSs the digraph $D_f(\mathcal{S})$ is strongly connected.

Lemma 5. *Consider a LETS \mathcal{S} with an irreducible transition matrix \mathbf{A} for flooding schedule. If after the construction of $D_l(\mathcal{S})$ from $D_f(\mathcal{S})$, all the nodes with no outgoing edges, and their incoming edges are removed from $D_l(\mathcal{S})$, then the remaining digraph (if any) is strongly connected.*

Lemma 5 implies that the FNF of the transition matrix $\tilde{\mathbf{A}}_{J \rightarrow 1}$ of a layered decoder for a LETS with irreducible matrix \mathbf{A} has at most one irreducible diagonal block. The following Lemma proves that the number of irreducible blocks is exactly one.

Lemma 6. *The FNF of a layered decoder transition matrix $\tilde{\mathbf{A}}_{J \rightarrow 1}$ corresponding to a LETS, \mathcal{S} , with irreducible flooding transition matrix, \mathbf{A} , has one and only one irreducible diagonal block.*

Proof. From Proposition 1, we have $\rho(\tilde{\mathbf{A}}_{J \rightarrow 1}) \geq \rho(\mathbf{A})$. Moreover, since \mathbf{A} is irreducible, $\rho(\mathbf{A}) > 1$ [45]. This means $\rho(\tilde{\mathbf{A}}_{J \rightarrow 1}) > 1$, and thus the FNF of $\tilde{\mathbf{A}}_{J \rightarrow 1}$ must have at least one irreducible diagonal block. This together with Lemma 5 completes the proof. ■

Based on Lemma 6, there exists a permutation matrix \mathbf{P} such that the FNF of $\tilde{\mathbf{A}}_{J \rightarrow 1}$ can be written as follows

$$\mathbf{P} \tilde{\mathbf{A}}_{J \rightarrow 1} \mathbf{P}^T = \left[\begin{array}{c|c} \mathbf{0}_{n_z \times n_z} & \tilde{\mathbf{A}}'_{n_z \times (m_s - n_z)} \\ \hline \mathbf{0}_{(m_s - n_z) \times n_z} & \tilde{\mathbf{A}}_{(m_s - n_z) \times (m_s - n_z)} \end{array} \right], \quad (46)$$

where $\tilde{\mathbf{A}}$ is a non-negative irreducible matrix and n_z is defined in Lemma 4.

Theorem 5. *Let $\tilde{\mathbf{A}}_{J \rightarrow 1}$ be the non-negative transition matrix of a LETS, which is not a simple cycle, in a layered decoder. Also, let the matrix $\tilde{\mathbf{A}}$ be the only irreducible diagonal block of the FNF of $\tilde{\mathbf{A}}_{J \rightarrow 1}$. Then,*

- (a) $\tilde{\mathbf{A}}_{J \rightarrow 1}$ has a simple positive eigenvalue, $\tilde{r} > 1$, equal to its spectral radius $\rho(\tilde{\mathbf{A}}_{J \rightarrow 1})$.

- (b) To \tilde{r} , there corresponds a non-negative left eigenvector $\tilde{\mathbf{w}}_1^T$ that is equal to the positive left eigenvector of $\tilde{\mathbf{A}}$, denoted by $\tilde{\omega}_1^T$, appended by n_z zeros.
- (c) To \tilde{r} , there corresponds a non-negative right eigenvector $\tilde{\mathbf{u}}_1$ that is equal to the positive right eigenvector of $\tilde{\mathbf{A}}$, denoted by $\tilde{\nu}_1$, appended by the vector $\frac{\tilde{\mathbf{A}}'}{\tilde{r}}\tilde{\nu}_1$, in which the matrix $\tilde{\mathbf{A}}'$ is defined in (46).

Proof. (a) The eigenvalues of $\tilde{\mathbf{A}}_{J \rightarrow 1}$ are the roots of $\det(\tilde{\mathbf{A}}_{J \rightarrow 1} - \mu \mathbf{I})$, which based on (46) simplifies to $\det(\tilde{\mathbf{A}} - \mu \mathbf{I})\mu^{n_z}$. The eigenvalues of irreducible matrix $\tilde{\mathbf{A}}$ together with n_z zeros are thus the eigenvalues of $\tilde{\mathbf{A}}_{J \rightarrow 1}$. Since, for a LETS that is not a simple cycle, $\tilde{\mathbf{A}}$ is a non-negative irreducible matrix, its dominant eigenvalue, \tilde{r} , which is positive and simple, is the dominant eigenvalue of $\tilde{\mathbf{A}}_{J \rightarrow 1}$ as well. Based on the proof of Lemma 6, this eigenvalue is larger than one, i.e., $\tilde{r} > 1$.

(b) Based on (46), to find the left eigenvector, $\tilde{\mathbf{w}}_1^T$, corresponding to \tilde{r} , we need to solve

$$\tilde{\mathbf{w}}_1^T \left[\begin{array}{c|c} \mathbf{0}_{n_z \times n_z} & \tilde{\mathbf{A}}'_{n_z \times (m_s - n_z)} \\ \hline \mathbf{0}_{(m_s - n_z) \times n_z} & \tilde{\mathbf{A}}_{(m_s - n_z) \times (m_s - n_z)} \end{array} \right] = \tilde{r} \tilde{\mathbf{w}}_1^T. \quad (47)$$

The solution to the above equation is a vector of the form

$$\tilde{\mathbf{w}}_1^T = \left[\mathbf{0}_{1 \times n_z} \mid \tilde{\omega}_1^T \right], \quad (48)$$

where $\tilde{\omega}_1^T$ is the positive left eigenvector of $\tilde{\mathbf{A}}$ corresponding to \tilde{r} .

(c) Similar to the proof of part (b), it can be easily shown that the right eigenvector of the FNF of $\tilde{\mathbf{A}}_{J \rightarrow 1}$ is

$$\tilde{\mathbf{u}}_1 = \left[\begin{array}{c} \frac{\tilde{\mathbf{A}}'}{\tilde{r}} \tilde{\nu}_1 \\ \tilde{\nu}_1 \end{array} \right]. \quad (49)$$

■

Example 9. The matrices $\tilde{\mathbf{A}}$ and $\tilde{\mathbf{A}}'$ in the FNF of the transition matrix of the $(5, 3)$ LETS of the Tanner code for the layered decoder are

$$\tilde{\mathbf{A}} = \begin{bmatrix} 0 & 0 & 0 & 1 & 0 & 0 & 0 \\ 0 & 0 & 0 & 0 & 1 & 0 & 1 \\ 1 & 0 & 0 & 0 & 0 & 1 & 0 \\ 1 & 0 & 0 & 0 & 0 & 1 & 1 \\ 0 & 1 & 0 & 0 & 0 & 1 & 0 \\ 0 & 0 & 1 & 0 & 1 & 0 & 0 \\ 0 & 1 & 0 & 1 & 0 & 0 & 0 \end{bmatrix}, \tilde{\mathbf{A}}' = \begin{bmatrix} 0 & 0 & 1 & 0 & 1 & 0 & 0 \\ 0 & 0 & 0 & 0 & 0 & 0 & 1 \\ 0 & 1 & 0 & 0 & 0 & 0 & 0 \\ 1 & 0 & 0 & 0 & 0 & 1 & 0 \\ 0 & 1 & 0 & 0 & 0 & 1 & 0 \end{bmatrix}.$$

The dominant eigenvalue of $\tilde{\mathbf{A}}$ is $\tilde{r} = 2.0136$, which is also equal to $\rho(\tilde{\mathbf{A}}_{3 \rightarrow 1})$. Moreover, the corresponding dominant left and right eigenvectors of the FNF of $\tilde{\mathbf{A}}_{3 \rightarrow 1}$ are

$$\tilde{\mathbf{w}}_1 = \begin{bmatrix} 0 \\ 0 \\ 0 \\ 0 \\ 0 \\ \hline 0.2838 \\ 0.4027 \\ 0.2525 \\ 0.3189 \\ 0.4525 \\ 0.5085 \\ 0.3584 \end{bmatrix}, \tilde{\mathbf{u}}_1 = \begin{bmatrix} 0.3342 \\ 0.2355 \\ 0.2096 \\ 0.2974 \\ 0.3756 \\ \hline 0.2647 \\ 0.4220 \\ 0.2974 \\ 0.5329 \\ 0.3756 \\ 0.3342 \\ 0.4743 \end{bmatrix}.$$

The lower partition of the left and right eigenvectors are equal to $\tilde{\omega}_1$ and $\tilde{\nu}_1$, the left and right eigenvectors of $\tilde{\mathbf{A}}$, respectively. Moreover, the upper partition of $\tilde{\mathbf{w}}_1$ is extended by $n_z = 5$ zeros while the upper part of $\tilde{\mathbf{u}}_1$ is equal to $\frac{\tilde{\mathbf{A}}'}{2.0136} \tilde{\nu}_1$.

In the following, to complement the result of Theorem 5, we discuss the case of LETSs that are simple cycles.

Theorem 6. Consider a simple cycle \mathcal{S} of length $2a$, and let \mathbf{A} and $\tilde{\mathbf{A}}_{J \rightarrow 1}$ denote the non-negative transition matrices of \mathcal{S} for flooding and layered decoders, respectively. Then

- (a) The FNF of $\tilde{\mathbf{A}}_{J \rightarrow 1}$ has two irreducible diagonal blocks.
- (b) $\tilde{r} = 1$ is an eigenvalue of $\tilde{\mathbf{A}}_{J \rightarrow 1}$, whose right eigenvector $\tilde{\mathbf{u}}_1$ is the same as the right eigenvector of \mathbf{A} , and whose left eigenvector, $\tilde{\mathbf{w}}_1^T$, is an all-one vector of length $2a - n_z$ appended by n_z zeros (up to a permutation), where n_z is the number of zero columns of $\tilde{\mathbf{A}}_{J \rightarrow 1}$.

Proof. (a) The flooding digraph $D_f(\mathcal{S})$ of the simple cycle \mathcal{S} consists of two disconnected directed cycles in opposite directions [45]. By the construction of $D_l(\mathcal{S})$ from $D_f(\mathcal{S})$, each of the directed cycles will be transformed into a new directed cycle, that is strongly connected, and thus corresponds to an irreducible diagonal block in the FNF of $\tilde{\mathbf{A}}_{J \rightarrow 1}$. In fact, the FNF of $\tilde{\mathbf{A}}_{J \rightarrow 1}$ has the following structure

$$\left[\begin{array}{c|cc} \mathbf{0} & & \tilde{\mathbf{A}}' \\ \hline & \tilde{\mathbf{A}}_{1(a-n_{z_1}) \times (a-n_{z_1})} & \mathbf{0} \\ \hline \mathbf{0} & \mathbf{0} & \tilde{\mathbf{A}}_{2(a-n_{z_2}) \times (a-n_{z_2})} \end{array} \right]_{2a \times 2a},$$

in which $\tilde{\mathbf{A}}_1$ and $\tilde{\mathbf{A}}_2$ are the irreducible blocks corresponding to the two directed cycles in opposite directions.

(b) It is known that for a simple cycle \mathcal{S} , the dominant eigenvalue of \mathbf{A} is $r = 1$ with multiplicity 2 [45]. It can be seen that Equation (44) is also applicable to simple cycles. Replacing $r = 1$ in (44) indicates that a right eigenvector \mathbf{u}_1 of \mathbf{A} corresponding to $r = 1$ is also a right eigenvector of $\tilde{\mathbf{A}}_{J \rightarrow 1}$ corresponding to $\tilde{r} = 1$. In fact, the eigenvalue $\tilde{r} = 1$ is the dominant eigenvalue of $\tilde{\mathbf{A}}_{J \rightarrow 1}$ with multiplicity 2. (Each of the diagonal blocks $\tilde{\mathbf{A}}_1$ and $\tilde{\mathbf{A}}_2$ has one dominant eigenvalue $\tilde{r} = 1$.) The all-one vectors with sizes $a - n_{z_1}$ and $a - n_{z_2}$ are the left eigenvectors of $\tilde{\mathbf{A}}_1$ and $\tilde{\mathbf{A}}_2$, respectively [45]. It is then easy to see that an all-one vector with size $2a - n_{z_1} - n_{z_2}$ appended by $n_z = n_{z_1} + n_{z_2}$ zeros is a left eigenvector of $\tilde{\mathbf{A}}_{J \rightarrow 1}$ (up to a permutation). ■

V. CALCULATION OF THE FAILURE PROBABILITY OF A LETS AND THE IMPACT OF ROW BLOCK PERMUTATIONS

In Subsection V-A, we calculate the error probability of a LETS using the linear state-space model. The effect of row block permutations on the error probability of a LETS is then studied in Subsection V-B. We end this section by proposing a two-step search algorithm in Subsection V-C to find a row block permutation that minimizes the error floor.

A. Computing the Failure Probability of LETSs in Layered Decoders

As the error indicator function, we consider the projection of the state vector, given in (30), onto the non-negative left eigenvector $\tilde{\mathbf{w}}_1^T$ of $\tilde{\mathbf{A}}_{J \rightarrow 1}$ corresponding to the dominant eigenvalue \tilde{r} :

$$\tilde{\beta}^{(\ell)} \triangleq \tilde{\mathbf{w}}_1^T \tilde{\mathbf{x}}^{(\ell)} = \gamma_{ch}^T \mathbf{L} + \sum_{i'=1}^{\ell} (\gamma_{ex}^{(i')T} \mathbf{L}_{ex}^{(i'-1)} + \gamma_{ex}^{(i')T} \mathbf{L}_{ex}^{(i')}), \quad (50)$$

in which the vectors γ_{ch}^T , $\gamma_{ex}^{\triangleleft(i')T}$ and $\gamma_{ex}^{\triangleright(i')T}$ have lengths equal to a , b and b , respectively. These vectors are defined by

$$\gamma_{ch}^T = \tilde{\mathbf{w}}_1^T \sum_{i=1}^{\ell} \left(\prod_{j=i+1}^{\ell} \tilde{\mathbf{A}}_{J \rightarrow 1}^{(j)} \right) \tilde{\mathbf{B}}^{(i)}, \quad (51)$$

$$\gamma_{ex}^{\triangleleft(i')T} = \tilde{\mathbf{w}}_1^T \left(\prod_{j'=i'+1}^{\ell} \tilde{\mathbf{A}}_{J \rightarrow 1}^{(j')} \right) \mathbf{B}_{ex}^{\triangleleft(i')} \quad i' = 1, \dots, \ell, \quad (52)$$

$$\gamma_{ex}^{\triangleright(i')T} = \tilde{\mathbf{w}}_1^T \left(\prod_{j'=i'+1}^{\ell} \tilde{\mathbf{A}}_{J \rightarrow 1}^{(j')} \right) \mathbf{B}_{ex}^{\triangleright(i')} \quad i' = 1, \dots, \ell. \quad (53)$$

The mean and variance of $\tilde{\beta}^{(\ell)}$ are calculated as

$$\mathbb{E}[\tilde{\beta}^{(\ell)}] = (2/\sigma_{ch}^2) \sum_{k=1}^a (\gamma_{ch}^T)_k + \sum_{i'=1}^{\ell-1} \left(\gamma_{ex}^{\triangleleft(i'+1)T} + \gamma_{ex}^{\triangleright(i')T} \right) \mathbf{m}_{ex}^{(i')} + \gamma_{ex}^{\triangleright(\ell)T} \mathbf{m}_{ex}^{(\ell)}, \quad (54)$$

and

$$\begin{aligned} \text{VAR}[\tilde{\beta}^{(\ell)}] &= (4/\sigma_{ch}^2) \sum_{k=1}^a (\gamma_{ch}^T)_k^2 \\ &+ \sum_{i'=1}^{\ell-1} \left(\gamma_{ex}^{\triangleleft(i'+1)T} + \gamma_{ex}^{\triangleright(i')T} \right) \Sigma_{ex}^{(i')} \left(\gamma_{ex}^{\triangleleft(i'+1)T} + \gamma_{ex}^{\triangleright(i')T} \right) + \gamma_{ex}^{\triangleright(\ell)T} \Sigma_{ex}^{(\ell)} \gamma_{ex}^{\triangleright(\ell)}, \end{aligned} \quad (55)$$

respectively. The symbol $(\cdot)_k$ is used to represent the k th element of the vector inside the parentheses. The $b \times 1$ vector $\mathbf{m}_{ex}^{(i')}$ and the $b \times b$ matrix $\Sigma_{ex}^{(i')}$ are the mean and the covariance matrix of the inputs from the unsatisfied CNs at iteration i' , respectively. Since we assume that external inputs to the LETS are independent, the matrix $\Sigma_{ex}^{(i')}$ is diagonal. The mean and the variance of the inputs from unsatisfied CNs are calculated using DE. Also, the missatisfied CN gains are calculated based on DE, as explained in Subsection IV-D. These gains are utilized in iteration dependent gain matrices involved in Equations (26) to (29). Finally, the vector γ_{ch}^T in (51) as well as the set of vectors $\gamma_{ex}^{\triangleleft(i')T}$ and $\gamma_{ex}^{\triangleright(i')T}$ for $i' = 1, \dots, \ell$ in (52) and (53), respectively, are used in Equations (54) and (55) to find the mean and the variance of the error indicator function, respectively. Finally, assuming that $\tilde{\beta}^{(\ell)}$ is Gaussian, the failure probability of a LETS, \mathcal{S} , is obtained by

$$P_e(\mathcal{S}) = \lim_{\ell \rightarrow \infty} \Pr\{\tilde{\beta}^{(\ell)} < 0\} = \lim_{\ell \rightarrow \infty} Q\left(\frac{\mathbb{E}[\tilde{\beta}^{(\ell)}]}{\sqrt{\text{VAR}[\tilde{\beta}^{(\ell)}]}}\right). \quad (56)$$

In practice, the error probability, given above, converges rather fast within a few iterations.

Suppose that the set $\{\mathcal{T}_i\}$ contains all the dominant LETSs of an LDPC code. Let \mathcal{E}_i denote the event that the decoder is failed due to \mathcal{T}_i . To estimate the error floor of the LDPC code, we partition $\{\mathcal{T}_i\}$ in accordance with the TSLP of TSs. This implies that within each class of LETSs, we first identify different non-isomorphic structures and then among those LETSs with the same structure, we identify different TSLPs. We then accordingly partition the class into different *groups*, where all the LETSs within a group have the same TSLP. Suppose that \mathcal{S}_i is the representative of the i th TS group with the size Υ_i . (Note that having the same TSLP implies that all the LETSs within a group have the same system matrices.) We then have the following approximation for the error floor of the code:

$$P_f \approx P\left(\bigcup_i \mathcal{E}_i\right) \lesssim \sum_i \Upsilon_i P_e(\mathcal{S}_i), \quad (57)$$

where the last step follows from the union bound.

We recall that for a LETS \mathcal{S} with an irreducible flooding transition matrix \mathbf{A} , all the elements of the left eigenvector of \mathbf{A} corresponding to the dominant eigenvalue r are positive. For the layered transition matrix $\tilde{\mathbf{A}}_{J \rightarrow 1}$, however, there are some zeros in the left eigenvector $\tilde{\mathbf{w}}_1^T$ corresponding to the dominant eigenvalue \tilde{r} . This implies that the corresponding state variables have no effect on the value of the error indicator function $\tilde{\beta}^{(\ell)}$. In fact, only the state variables corresponding to the irreducible part of the transition matrix $\tilde{\mathbf{A}}_{J \rightarrow 1}$ are the ones that determine the value of $\tilde{\beta}^{(\ell)}$, and are the main contributors to the growth of erroneous messages inside \mathcal{S} .

B. Effect of Different Row Block Permutations on the Dominant Eigenvalue of $\tilde{\mathbf{A}}_{J \rightarrow 1}$

In the asymptotic regime of $\ell \rightarrow \infty$, the dominant eigenvalue \tilde{r} of the transition matrix $\tilde{\mathbf{A}}_{J \rightarrow 1}$ plays an important role in the failure probability of a LETS in a layered decoder. The value of \tilde{r} can however change depending on the order in which different layers within the LETS are updated. To simplify the discussions, we assume that in the layered decoding, the row blocks of the parity check matrix are updated based on their increased indices, i.e., starting from the first row block all the way down to the row block number m_b . We thus associate the different orderings of row updates with different permutations of the row blocks of the parity-check matrix. In this part, we consider the effect of different row block permutations on \tilde{r} .

In general, for a LETS with J layers, there are $J!$ different layer permutations. We denote the set of all possible permutations of J layers by Π_J . A given permutation $\pi \in \Pi_J$ is identified by the sequence $\pi(1), \dots, \pi(J)$, or more briefly by π_1, \dots, π_J .

Proposition 2. Consider the application of a permutation π to the J layers of a LETS \mathcal{S} , and denote the corresponding transition matrix of \mathcal{S} in the layered decoder by $\tilde{\mathbf{A}}_{\pi_J \rightarrow \pi_1}$. The dominant eigenvalue of $\tilde{\mathbf{A}}_{\pi_J \rightarrow \pi_1}$ is then invariant to any cyclic shift of the permutation π .

Proof. Suppose that the right eigenvector of \tilde{r} for $\tilde{\mathbf{A}}_{\pi_J \rightarrow \pi_1}$ is $\tilde{\mathbf{u}}_1$. We then have

$$\underbrace{\mathcal{A}_{\pi_J} \mathcal{A}_{\pi_{J-1}} \dots \mathcal{A}_{\pi_1}}_{\tilde{\mathbf{A}}_{\pi_J \rightarrow \pi_1}} \tilde{\mathbf{u}}_1 = \tilde{r} \tilde{\mathbf{u}}_1.$$

Multiplying both sides of this equation sequentially with $\mathcal{A}_{\pi_1}, \mathcal{A}_{\pi_2}, \dots, \mathcal{A}_{\pi_{J-1}}$, results in

$$\begin{aligned} \underbrace{\mathcal{A}_{\pi_1} \mathcal{A}_{\pi_J} \dots \mathcal{A}_{\pi_2}}_{1 \text{ cyclic shift}} (\mathcal{A}_{\pi_1} \tilde{\mathbf{u}}_1) &= \tilde{r} (\mathcal{A}_{\pi_1} \tilde{\mathbf{u}}_1), \\ \underbrace{\mathcal{A}_{\pi_2} \mathcal{A}_{\pi_1} \mathcal{A}_{\pi_J} \dots \mathcal{A}_{\pi_3}}_{2 \text{ cyclic shifts}} (\mathcal{A}_{\pi_2} \mathcal{A}_{\pi_1} \tilde{\mathbf{u}}_1) &= \tilde{r} (\mathcal{A}_{\pi_2} \mathcal{A}_{\pi_1} \tilde{\mathbf{u}}_1), \\ &\vdots \\ \underbrace{\mathcal{A}_{\pi_{J-1}} \dots \mathcal{A}_{\pi_1} \mathcal{A}_{\pi_J}}_{J-1 \text{ cyclic shifts}} (\mathcal{A}_{\pi_{J-1}} \dots \mathcal{A}_{\pi_1} \tilde{\mathbf{u}}_1) &= \tilde{r} (\mathcal{A}_{\pi_{J-1}} \dots \mathcal{A}_{\pi_1} \tilde{\mathbf{u}}_1), \end{aligned}$$

respectively. As can be seen, \tilde{r} is the eigenvalue of all the transition matrices resulted from different cyclic shifts of the permutation π . The above equations can be written for all the eigenvalues of $\tilde{\mathbf{A}}_{\pi_J \rightarrow \pi_1}$, and thus, \tilde{r} remains the dominant eigenvalue of all such transition matrices. ■

In the following proposition, whose proof is given in the appendix, we prove that reversing the layer permutation does not change \tilde{r} .

Proposition 3. Consider the transition matrix $\tilde{\mathbf{A}}_{\pi_J \rightarrow \pi_1}$ of a LETS with J layers corresponding to a layer permutation π . Then, the eigenvalues of $\tilde{\mathbf{A}}_{\pi_J \rightarrow \pi_1}$ are invariant under the reversing of π , i.e., the transition matrix $\tilde{\mathbf{A}}_{\pi_1 \rightarrow \pi_J}$ corresponding to the reverse permutation π_J, \dots, π_1 has the same eigenvalues as $\tilde{\mathbf{A}}_{\pi_J \rightarrow \pi_1}$.

Based on Propositions 2 and 3, we have the following result.

Corollary 1. For a LETS with J layers ($J \geq 3$), the number of distinct dominant eigenvalues of the layered transition matrix corresponding to different permutations of the layers is upper bounded by $\frac{(J-1)!}{2}$.

Corollary 1 implies that for a LETS with three layers ($J = 3$), all the layered transition matrices corresponding to different layer permutations have the same dominant eigenvalue.

Example 10. *The Tanner (155, 64) LDPC code has 3 row layers, and based on Corollary 1, the dominant eigenvalue of the layered transition matrices of all of its LETSs are invariant under all the possible (6) layer permutations.*

C. Optimizing the Row Layered Schedule

The contribution of each LETS \mathcal{S} to the error floor of an LDPC code, decoded by a row layered iterative algorithm, depends on the distribution of messages entering \mathcal{S} through its missatisfied and unsatisfied CNs as well as the internal structure of \mathcal{S} . In the linear state-space model used in this work, the internal structure is reflected in the system matrices in general, and the transition matrix $\tilde{\mathbf{A}}_{J \rightarrow 1}$, in particular. More specifically, our results show that the dominant eigenvalue \tilde{r} of the transition matrix plays an important role in the growth rate of erroneous messages inside the subgraph of \mathcal{S} , with larger values of \tilde{r} generally corresponding to larger growth rate. As we discussed in Subsection V-B, however, the transition matrix $\tilde{\mathbf{A}}_{J \rightarrow 1}$ and \tilde{r} can change with layer permutations. Moreover, different layer permutations can result in notable change in the TSLP and thus the distributions of the external messages entering the TS. As a result, different row layered schedules can potentially produce error floors that are considerably different. This motivates the search for layer permutations which result in low error floors. In the following, we show that our proposed model can be used not only for the error floor estimation of layered decoders, but also as an efficient tool to find row layered schedules with low error floors.

Generally, for a given QC-LDPC code whose base matrix \mathbf{H}_b has m_b rows, there are $m_b!$ different row layered schedules corresponding to different row permutations of \mathbf{H}_b . The complexity of an exhaustive search among all such schedules based on the exact estimation of the error floor can be prohibitive for relatively large values of m_b . The main source of complexity in our model is to obtain the distribution of external messages by DE. (Recall that, for each iteration, $2|E_b|$ distributions are needed to be calculated, where $|E_b|$ is the number of edges in the base graph, which is equal to the number of nonzero elements of \mathbf{H}_b .) To simplify the search among the $m_b!$ different row layered schedules, rather than the derivation of such distributions for each schedule, we select one schedule, say the one corresponding to the original order of the rows, and then at each iteration ℓ and for each layer j , we derive the average distributions of CN to VN messages and VN to CN messages, denoted by $\overleftarrow{\psi}_\ell^j$ and $\overrightarrow{\psi}_\ell^j$, respectively, where the average is taken over all the corresponding distributions within layer L_j . These average distributions are then used to represent all the CN to VN and VN to CN distributions in the j th layer of decoding

regardless of the schedule. As an example, for the base graph of Fig. 3, the distribution $\bar{\psi}_\ell^3$ is the average of $\psi_\ell^{[2 \leftarrow 3]}$ and $\psi_\ell^{[4 \leftarrow 3]}$, and $\bar{\psi}_\ell^3$ is the average of $\psi_\ell^{[2 \rightarrow 3]}$ and $\psi_\ell^{[4 \rightarrow 3]}$.

The averaging process just explained will result in a less accurate estimate of the failure rate of a LETS. In fact, by ignoring the effect of scheduling in the distribution of external messages and by the averaging, we only observe the effect of the schedule on the internal messages of the LETS. To find the schedule with the lowest error floor, we then perform the search in two steps. In the first step, we use the above approximation/simplification and search among all the $m_b!$ schedules to find a few candidates that have lower error floors. In the second step, we examine the candidate schedules by calculating the error floor estimates accurately (by considering the effect of scheduling in the distribution of external messages), and find the one with the lowest error floor.

VI. SIMULATION RESULTS AND DISCUSSIONS

In this section, we investigate the accuracy of the proposed linear state-space model in estimating the error floor of row layered SPA through simulations. We consider two QC-LDPC codes \mathcal{C}_1 and \mathcal{C}_2 , whose exponent matrices are shown in Figs. 7a and 7b, respectively. \mathcal{C}_1 is a (640, 192) variable-regular code with $d_v = 5$ and irregular CN degrees [3] and \mathcal{C}_2 is a (576, 432) irregular code used in Wimax standard [76]. The lifting degrees for the two codes are 64 and 24, respectively.

The Monte Carlo simulation results as well as estimation results for the layered decoding of \mathcal{C}_1 where the order of row layers are the same as that of Fig. 7a, for different saturation levels are presented in Fig. 8. The most harmful structure of this code in the error floor region is the (5, 5) LETS, shown in Fig. 9, with multiplicity 64. All the (5, 5) LETSs have the same TSLP. As expected, by increasing the saturation level, the error floor is reduced. The figure also shows a good match between the linear model estimation results and simulation results. The slight over-estimation of error floor is attributed to the linear approximation of missatisfied CN operations (see [47], for more information).

We now investigate the effect of row block permutations on the error floor of \mathcal{C}_1 . \mathcal{C}_1 has 7 row layers, each corresponding to one of the row blocks of the parity-check matrix. We label these row blocks with numbers 1 to 7 based on their indices in Fig. 7a, i.e., the first row block in Fig. 7a is labeled by 1, the second by 2, and so on. We then represent different schedules with different permutations of numbers from 1 to 7. For example, permutation (1, 2, 3, 4, 5, 6, 7)

8	-1	26	62	-1	-1	59	19	-1	60
51	9	50	-1	39	-1	4	-1	25	26
-1	32	10	7	56	52	41	55	61	41
46	11	-1	43	-1	63	8	51	37	-1
47	7	7	50	49	53	-1	12	-1	-1
31	-1	-1	-1	31	38	-1	-1	23	48
-1	25	21	56	59	30	27	23	27	18

(a) Exponent matrix of \mathcal{C}_1 : (640, 192) QC-LDPC code with lifting degree 64.

-1	20	-1	7	-1	-1	3	6	4	-1	-1	21	7	13	19	23	5	23	0	0	-1	-1	-1	-1
10	-1	3	17	8	-1	-1	-1	-1	17	10	2	9	10	8	14	9	6	-1	0	0	-1	-1	-1
-1	-1	5	-1	-1	15	9	-1	17	16	-1	9	1	18	11	7	15	1	20	-1	0	0	-1	-1
16	0	-1	-1	15	-1	-1	0	12	-1	20	3	23	2	21	9	3	4	-1	-1	-1	0	0	-1
-1	13	15	20	-1	6	18	-1	-1	-1	-1	21	19	0	0	18	15	6	-1	-1	-1	-1	0	0
19	-1	-1	-1	3	7	-1	8	-1	18	7	17	21	21	6	16	2	22	0	-1	-1	-1	-1	0

(b) Exponent matrix of \mathcal{C}_2 : (576, 432) Wimax QC-LDPC code with lifting degree 24.

Fig. 7. QC-LDPC codes used for simulations. The entries of the matrices, that are not equal to -1 , represent the right circular shift of the identity matrix to create the corresponding block of the parity-check matrix. The -1 entries represent zero blocks.

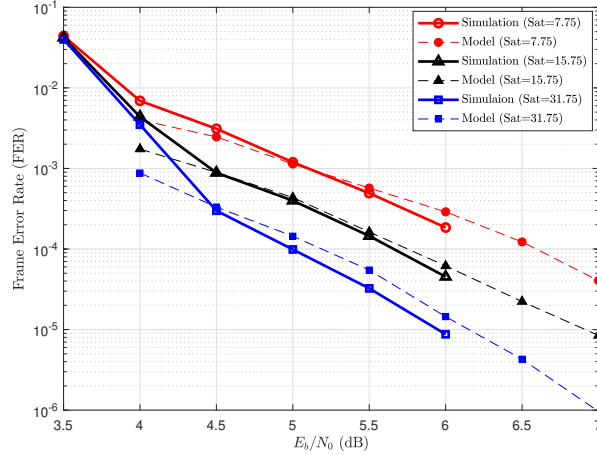


Fig. 8. Simulation and estimation results of \mathcal{C}_1 for different saturation levels. The maximum number of iterations $I_{max} = 30$.

corresponds to a schedule which updates the row layers in the same order as they appear in Fig. 7a.

In order to investigate the effect of different row schedules on the error floor performance of \mathcal{C}_1 , the technique of Section V-C is used. The total number of possible row permutations for \mathcal{C}_1 is $7! = 5040$. These permutations in general correspond to different system matrices for the (5, 5) LETS. By using a single application of DE, as discussed in Section V-C, the failure

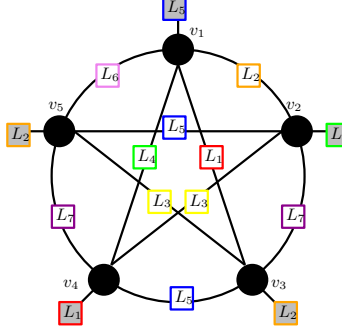


Fig. 9. The $(5, 5)$ LETS structure of \mathcal{C}_1 in which the row layers for different CNs are shown.

rate of the $(5, 5)$ LETS for different schedules is approximated. The results for SNR of 6 dB and saturation level of 31.75 are provided in Fig. 10 for all the schedules. As can be seen, the estimation results are partitioned into 8 groups, separated by vertical dotted lines. The transition matrices of the schedules within each group have the same dominant eigenvalue \tilde{r} . We have also sorted the groups according to the increasing value of \tilde{r} . The eight different values of \tilde{r} are shown in Fig. 10, and range from 12.402 to 16.125. Note that based on Corollary 1, the upper bound on the number of different \tilde{r} values for different schedules for the case where the LETS has 7 layers is 360, in general. Fig. 10 shows the trend that increasing \tilde{r} , on average, increases the failure probability of the LETS. Within each group, however, the variance of the error probabilities is still rather large. This implies that while \tilde{r} plays an important role in the failure probability of a LETS, there are also other factors, including the layering structure of the TS reflected through the system matrices, that affect the harmfulness. (Note that, in this analysis, although the distributions of the external messages of the LETS for different layers, obtained through DE, remains constant for different schedules, but the assignment of different CNs and VNs of the LETS to different layers will change due to the change of schedule. As a result, the distributions of messages associated with these nodes will also change in different schedules.)

To find a schedule with low error floor, in the next step, we select a few schedules whose transition matrices have the minimum dominant eigenvalue, $\tilde{r} = 12.402$, and result in the lowest error rates in the first step. We then apply our estimation technique accurately to find the error floor of these candidate schedules, and select the one that has the lowest error floor. As a result, we obtain the schedule corresponding to the permutation $(2, 3, 1, 7, 4, 5, 6)$, shown in Fig. 10 with a full diamond. For comparison, we have also selected one of the schedules with the worst error floor, $(4, 6, 5, 7, 3, 1, 2)$, as well as the original one, $(1, 2, 3, 4, 5, 6, 7)$. These schedules are

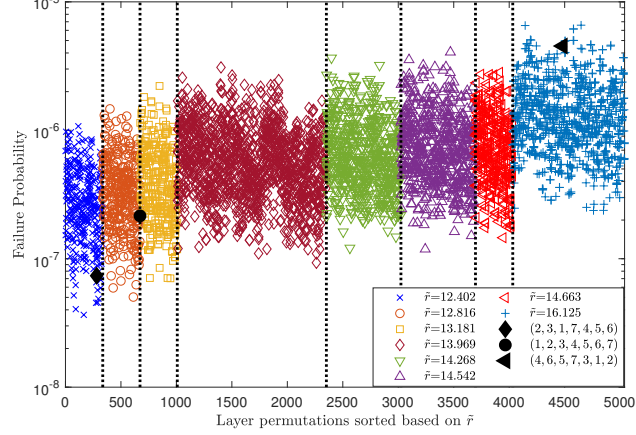


Fig. 10. The approximate estimate of the failure probability of the $(5, 5)$ LETS of \mathcal{C}_1 for various row layered schedules at $E_b/N_0 = 6$ dB and saturation level 31.75. The schedules are sorted based on \tilde{r} .

specified in Fig. 10 by a full triangle and a full circle, respectively. The simulation and estimation results of these three schedules are presented in Fig. 11. The maximum number of iterations and the saturation level are $I_{max} = 30$ and 31.75, respectively. For comparison, we have also included the FER of the flooding schedule with maximum number of iterations $I_{max} = 60$ in Fig. 11. As can be seen, all the estimation results match closely with the corresponding simulations. Remarkably, there is a substantial difference between the FER of the best and worst layered schedules in the error floor region, with the performance of flooding schedule in the middle. This demonstrates the gain that one can obtain in performance by properly choosing the updating order of layers in a layered decoder, basically at no cost. It also shows that a layered decoder can, in general, have a better or a worse performance compared to its flooding counterpart. By proper permutation of row layers, the layered decoder not only has a faster convergence speed compared to a flooding decoder but also can have a better performance.

As the next example, we consider \mathcal{C}_2 . The multiplicity of different (a, b) LETSs of this code within the range $a \leq 8$ and $b \leq 2$ are listed in Table III. These LETSs have been found using the exhaustive search algorithm of [32]. As can be seen, this code has a variety of LETSs that can potentially contribute to the error floor performance. Moreover, unlike the previous example, there are different non-isomorphic structures within each class of TSs. For example, there are 8 different non-isomorphic $(7, 1)$ LETS structures in this code. For 2 out of 8 structures, the code also contains TSs with two different TSLPs. This means that there are ten $(7, 1)$ LETS groups, each with size 24, that can have different failure probabilities under a layered decoder.

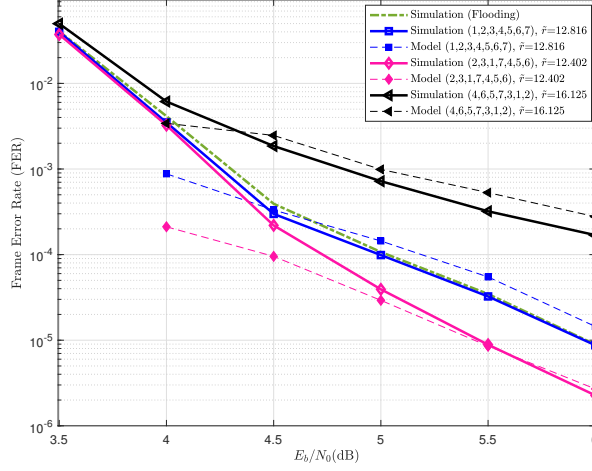


Fig. 11. The simulation and estimation results of \mathcal{C}_1 for different row schedules. (The saturation level is 31.75, and the maximum number of iterations for layered schedules and the flooding schedule are set to 30 and 60, respectively.)

TABLE III
MULTIPLICITIES OF (a, b) LETSS OF \mathcal{C}_2 WITHIN THE RANGE $a \leq 8$ AND $b \leq 2$

(a, b)	(4, 2)	(5, 2)	(6, 1)	(6, 2)	(7, 1)	(7, 2)	(8, 0)	(8, 1)	(8, 2)
Multiplicity	144	216	48	1068	240	3600	48	720	13464

We denote these groups by $(7, 1)_1, \dots, (7, 1)_{10}$, respectively.

To evaluate the effect of row scheduling on the error floor of \mathcal{C}_2 , the same general technique as the one employed in the previous example is used. In this regard, for each of the LETS groups (those with the same structure and TSLP) within $(6, 1)$, $(7, 1)$, $(8, 0)$ and $(8, 1)$ classes, we estimate the failure probability of various schedules. This is performed based on the approximate average DE method of Subsection V-C at $E_b/N_0 = 6$ dB and for a saturation level of 15.75. The number of LETS groups within each of the aforementioned classes are 2, 10, 2 and 30, respectively. Each group has the same size of 24. To estimate the contribution of each LETS class to the error floor, we first estimate the failure rate of a member of each LETS group within the class, then multiply the result by 24, and finally add up the results for different groups within the class. These results for different classes are presented in Fig. 12, for all the $6! = 720$ possible row schedules. As can be observed, on average, the most harmful LETS class of this code, for saturation level 15.75, is the $(7, 1)$ class. In order to observe the overall error probability for different row schedules, the contribution of different classes from Fig. 12 are added and presented

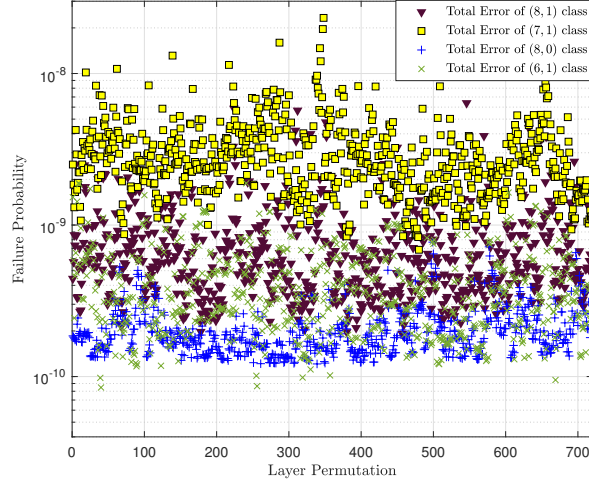


Fig. 12. The effect of various row layered schedules on the failure probability of different classes of LETSs in \mathcal{C}_2 ($E_b/N_0 = 6$ dB, saturation level 15.75).

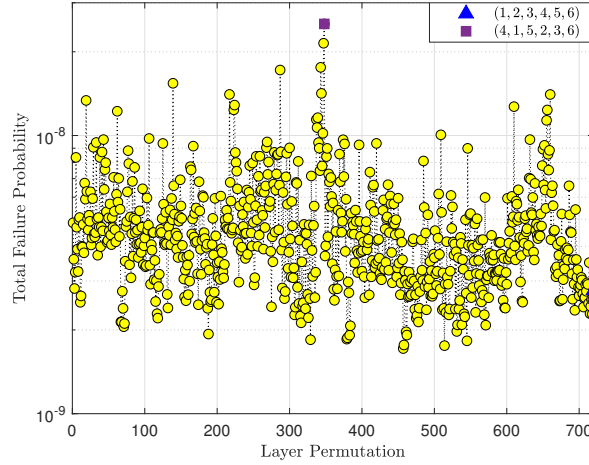


Fig. 13. The effect of various row layered schedules on the total FER of \mathcal{C}_2 ($E_b/N_0 = 6$ dB, saturation level 15.75).

in Fig. 13. Interestingly, for \mathcal{C}_2 , it appears that the original schedule (1, 2, 3, 4, 5, 6) has one of the lowest error rates. This schedule is shown in Fig. 13 by a full triangle. The worst schedule in Fig. 13 is (4, 1, 5, 2, 3, 6), and is identified by a full square.

For the two schedules (1, 2, 3, 4, 5, 6) and (4, 1, 5, 2, 3, 6), we have estimated the failure probability of each of the 10 LETS groups within the class (7, 1), using the exact DE. These results along with the total failure probability of the (7, 1) class are provided in Fig. 14. We note that the LETSs within first and third groups, i.e., $(7, 1)_1$ and $(7, 1)_3$, are isomorphic (they only differ

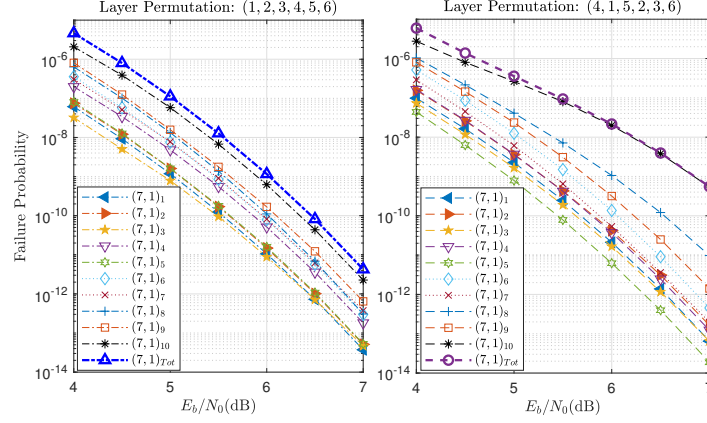


Fig. 14. The error estimation of the ten $(7, 1)$ LETS groups of \mathcal{C}_2 for the two schedules $(1, 2, 3, 4, 5, 6)$ and $(4, 1, 5, 2, 3, 6)$ (saturation level 15.75).

by their TSLPs). So are the LETSs within $(7, 1)_6$ and $(7, 1)_7$. The examination of Fig. 14 for schedule $(4, 1, 5, 2, 3, 6)$ shows that the two groups $(7, 1)_6$ and $(7, 1)_7$, despite having the same structure, have different error probabilities, due to different TSLPs. Fig. 14 also demonstrates that, for both schedules, the LETS group $(7, 1)_{10}$ is the most harmful one. The LETS structure of $(7, 1)_{10}$ has 6 layers and in fact, if one considers all the possible layer permutations, this structure has 57 different \tilde{r} values. This is close to the upper bound of 60 from Corollary 1. The 57 different \tilde{r} values for the $(7, 1)_{10}$ structure are between 6.043 and 8.216. For the two schedules $(1, 2, 3, 4, 5, 6)$ and $(4, 1, 5, 2, 3, 6)$, these values are 6.408 and 8.216, respectively. Another observation from Fig. 14 is that the relative harmfulness of the TSs can change depending on the schedule. For example, while the $(7, 1)_8$ is the second most harmful group of LETSs for schedule $(4, 1, 5, 2, 3, 6)$, for $(1, 2, 3, 4, 5, 6)$, the second most harmful group is $(7, 1)_9$.

In order to examine the accuracy of our estimations, the simulation results for the two schedules together with the estimation results based on the contributions of $(6, 1)$, $(7, 1)$, $(8, 0)$ and $(8, 1)$ LETS classes are shown in Fig. 15. As can be seen, for both schedules, there is a good match between simulations and estimations.

Finally, in our experiments, we observe that the same row layered schedule that minimizes the error floor of SPA also performs well for min-sum algorithm (MSA). This is explained in Fig. 16 for \mathcal{C}_1 , where we have used row layered MSA (saturation level 31.75, maximum number of iterations 30) with the same three schedules as in Fig. 11. As can be seen, the three

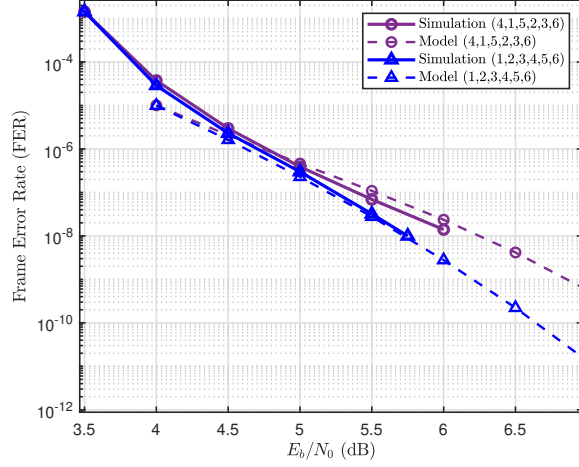


Fig. 15. Simulation and estimation results of \mathcal{C}_2 for the two schedules (1, 2, 3, 4, 5, 6) and (4, 1, 5, 2, 3, 6) (saturation level 15.75, $I_{max} = 30$).

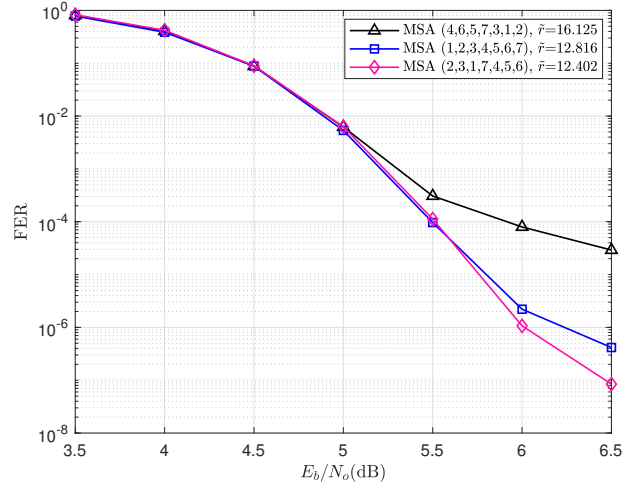


Fig. 16. Performance of \mathcal{C}_1 under row layered MSA with row schedules similar to those of Fig. 11 (the saturation level and the maximum number of iterations are 31.75 and 30, respectively.)

schedules have the same relative performance as they had with SPA. In particular, the schedule (2, 3, 1, 7, 4, 5, 6) that was optimal for SPA still performs the best with MSA.

VII. CONCLUSION

In this paper, we studied the error floor of QC-LDPC codes under row layered saturating SPA. For this, we developed a linear state-space model for LETSs of the code which incorporates the layered nature of scheduling. We then studied the system matrices of the model and made

connections between these matrices and those corresponding to the linear state-space model of the flooding decoder. In particular, we demonstrated that the spectral radius of the transition matrix of the layered decoder is always larger than that of its flooding counterpart.

We showed that the proposed model can estimate the failure probability of LETSs, as well as the error floor of the code rather accurately. In particular, we demonstrated that the failure rate of a LETS under layered decoding is not only a function of its topology, but also depends on the location of its constituent CNs in different layers. We called this information, TS layer profile, or TSLP, in brief. As a result, we established that the error floor of the same code under the same saturating SPA can significantly change by modifying the order in which the row layers are updated. We also studied the problem of finding the schedule with the lowest error floor and devised an efficient algorithm to find it. In particular, we demonstrated that the layered decoder, with a well designed schedule, can outperform its flooding counterpart. This adds yet another advantage to the application of layered decoding in practice. The well-known advantages, prior to this result, were the faster convergence and lower hardware complexity.

We note that the linear state-space model presented in this paper can also be applied to column layered decoders [77], [78]. The application however involves non-trivial modifications to derive the model parameters.

For the codes studied in this work, the vast majority of problematic TSs were LETSs. We however note that the linear state-space model can also be applied to ETSs with leaf, if such TSs happen to have a non-negligible contribution to the error floor.

An interesting line of inquiry would be to use the results of this work in the design of QC-LDPC codes with low error floor under layered decoding.

VIII. APPENDIX: PROOF OF PROPOSITION 3

To prove Proposition 3, we first need the following lemmas.

Lemma 7. *Consider the linear state-space model of a LETS in which the two state variables corresponding to each missatisfied CN are labeled by consecutive numbers, and let \mathbf{A} be the corresponding flooding transition matrix. We then have*

- (a) *If $\mathbf{A}(i, j) = 1$, then $\mathbf{A}(j + 2 \times \text{mod}(j, 2) - 1, i + 2 \times \text{mod}(i, 2) - 1) = 1$, where $\text{mod}(i, 2)$ is used to denote the value of i modulo 2.*

(b) If the nonzero entries of an $m_s \times m_s$ symmetric and unitary permutation matrix \mathbf{P} are defined by $\mathbf{P}(i, i + 2 \times \text{mod}(i, 2) - 1) = 1$, for $i = 1, \dots, m_s$, then

$$\mathbf{A}^T = \mathbf{PAP}. \quad (58)$$

Proof. (a) To each missatisfied CN, there correspond two state variables with even and odd labels, respectively. Denoting the state variables of a given missatisfied CN by x_{2k} and x_{2k-1} , one can see that each of them is a function of at least one other state variable corresponding to another missatisfied CN. Suppose that x_{2k} is a function of state variable $x_{2k'}$ (or $x_{2k'-1}$) from another missatisfied CN. Then, $x_{2k'-1}$ (or $x_{2k'}$) must be a function of x_{2k-1} . This corresponds to the relationship between the entries of \mathbf{A} as described in Part (a) of the lemma. (b) The symmetric application of the permutation matrix \mathbf{P} to \mathbf{A} , i.e., \mathbf{PAP}^T , permutes the even and odd rows and columns that correspond to each missatisfied CN. Based on the result of Part (a), this permutation results in the transpose matrix \mathbf{A}^T . Also, Equation (58) is derived based on the fact that $\mathbf{P}^T = \mathbf{P}$. ■

Lemma 8. Let μ_k and \mathbf{u}_k be an eigenvalue and its corresponding right eigenvector of a layered transition matrix $\tilde{\mathbf{A}}_{J \rightarrow 1}$, which is in systematic form. Then,

$$(\mu_k \mathbf{A}_l + \mathbf{A}_u) \mathbf{u}_k = \mu_k \mathbf{u}_k, \quad (59)$$

where \mathbf{A}_l and \mathbf{A}_u are the lower and upper triangular parts of the corresponding flooding transition matrix $\mathbf{A} = \mathbf{A}_l + \mathbf{A}_u$.

Proof. For simplicity, we prove the result for a LETS with $J = 3$ layers. The proof for larger values of J is similar. By the definition of an eigenvalue and the corresponding eigenvector, we have

$$\tilde{\mathbf{A}}_{3 \rightarrow 1} \begin{bmatrix} \mathbf{u}_{k,1} \\ \mathbf{u}_{k,2} \\ \mathbf{u}_{k,3} \end{bmatrix} = \mu_k \begin{bmatrix} \mathbf{u}_{k,1} \\ \mathbf{u}_{k,2} \\ \mathbf{u}_{k,3} \end{bmatrix},$$

in which the eigenvector is partitioned according to the three layers. By replacing $\tilde{\mathbf{A}}_{3 \rightarrow 1}$ in the

above equation with the sub-matrices from (40), we can write

$$\begin{aligned}
& \mathbf{A}_{1,2}\mathbf{u}_{k,2} + \mathbf{A}_{1,3}\mathbf{u}_{k,3} = \mu_k\mathbf{u}_{k,1}, \\
& \mathbf{A}_{2,1}(\underbrace{\mathbf{A}_{1,2}\mathbf{u}_{k,2} + \mathbf{A}_{1,3}\mathbf{u}_{k,3}}_{\mu_k\mathbf{u}_{k,1}}) + \mathbf{A}_{2,3}\mathbf{u}_{k,3} = \mu_k\mathbf{u}_{k,2}, \\
& \mathbf{A}_{3,1}(\underbrace{\mathbf{A}_{1,2}\mathbf{u}_{k,2} + \mathbf{A}_{1,3}\mathbf{u}_{k,3}}_{\mu_k\mathbf{u}_{k,1}}) + \\
& \mathbf{A}_{3,2}(\underbrace{\mathbf{A}_{2,1}(\mathbf{A}_{1,2}\mathbf{u}_{k,2} + \mathbf{A}_{1,3}\mathbf{u}_{k,3}) + \mathbf{A}_{2,3}\mathbf{u}_{k,3}}_{\mu_k\mathbf{u}_{k,2}}) = \mu_k\mathbf{u}_{k,3},
\end{aligned}$$

or equivalently,

$$\underbrace{\begin{bmatrix} \mathbf{0} & \mathbf{A}_{1,2} & \mathbf{A}_{1,3} \\ \mu_k\mathbf{A}_{2,1} & \mathbf{0} & \mathbf{A}_{2,3} \\ \mu_k\mathbf{A}_{3,1} & \mu_k\mathbf{A}_{3,2} & \mathbf{0} \end{bmatrix}}_{(\mu_k\mathbf{A}_l + \mathbf{A}_u)} \begin{bmatrix} \mathbf{u}_{k,1} \\ \mathbf{u}_{k,2} \\ \mathbf{u}_{k,3} \end{bmatrix} = \mu_k \begin{bmatrix} \mathbf{u}_{k,1} \\ \mathbf{u}_{k,2} \\ \mathbf{u}_{k,3} \end{bmatrix},$$

which is the same as (59) for $J = 3$. ■

The proof of the following lemma is similar to that of Lemma 8.

Lemma 9. Let $\tilde{\mathbf{A}}_{1 \rightarrow J} = \mathcal{A}_1 \mathcal{A}_2 \cdots \mathcal{A}_J$ be the systematic layered transition matrix of a LETS for the row layered decoder in which the order of layers is reversed. Also, let μ'_k and \mathbf{u}'_k be an eigenvalue and its corresponding right eigenvector of $\tilde{\mathbf{A}}_{1 \rightarrow J}$. Then

$$(\mathbf{A}_l + \mu'_k \mathbf{A}_u) \mathbf{u}'_k = \mu'_k \mathbf{u}'_k, \quad (60)$$

where \mathbf{A}_l and \mathbf{A}_u are the lower and upper triangular part of the corresponding flooding transition matrix $\mathbf{A} = \mathbf{A}_l + \mathbf{A}_u$.

To prove Proposition 3, without loss of generality, we assume that $\tilde{\mathbf{A}}_{\pi_J \rightarrow \pi_1}$ is in the systematic form. Then, according to Lemma 8, for $\tilde{\mathbf{A}}_{\pi_J \rightarrow \pi_1}$, we have

$$(\tilde{r}_i \mathbf{A}_l + \mathbf{A}_u) \tilde{\mathbf{u}}_i = \tilde{r}_i \tilde{\mathbf{u}}_i,$$

where \tilde{r}_i and $\tilde{\mathbf{u}}_i$ are an eigenvalue and its corresponding eigenvector of $\tilde{\mathbf{A}}_{\pi_J \rightarrow \pi_1}$, respectively. Suppose that \mathbf{P} is the permutation matrix defined in Lemma 7. Since $\mathbf{P}\mathbf{P} = \mathbf{I}$, we can write

$$(\tilde{r}_i \mathbf{A}_l \mathbf{P} + \mathbf{A}_u \mathbf{P}) \mathbf{P} \tilde{\mathbf{u}}_i = \tilde{r}_i \tilde{\mathbf{u}}_i. \quad (61)$$

Moreover, for a systematic flooding transition matrix \mathbf{A} , one can show that $\mathbf{A}_l \mathbf{P} = \mathbf{P} \mathbf{A}_u^T$ and $\mathbf{A}_u \mathbf{P} = \mathbf{P} \mathbf{A}_l^T$. Using these in (61), we obtain

$$(\mathbf{P} \mathbf{A}_l^T + \tilde{r}_i \mathbf{P} \mathbf{A}_u^T) \mathbf{P} \tilde{\mathbf{u}}_i = \tilde{r}_i \tilde{\mathbf{u}}_i. \quad (62)$$

Multiplying both sides by \mathbf{P} results in

$$(\mathbf{A}_l + \tilde{r}_i \mathbf{A}_u)^T \mathbf{P} \tilde{\mathbf{u}}_i = \tilde{r}_i \mathbf{P} \tilde{\mathbf{u}}_i. \quad (63)$$

From (63), the eigenvalues \tilde{r}_i are the roots of the following equation:

$$\det[(\mathbf{A}_l + \tilde{r}_i \mathbf{A}_u)^T - \tilde{r}_i \mathbf{I}] = \det[(\mathbf{A}_l + \tilde{r}_i \mathbf{A}_u) - \tilde{r}_i \mathbf{I}] = 0. \quad (64)$$

On the other hand, based on Lemma 9, the roots of the determinant on the right hand side are the eigenvalues of $\tilde{\mathbf{A}}_{\pi_1 \rightarrow \pi_J}$. This completes the proof.

REFERENCES

- [1] E. Cavus and B. Daneshrad, "A performance improvement and error floor avoidance technique for belief propagation decoding of LDPC codes," in *Proc. 16th IEEE Int. Symp. Personal, Indoor Mobile Radio Commun.*, Los Angeles, CA, USA, Sep. 2005, pp. 2386–2390.
- [2] Y. Han and W. E. Ryan, "LDPC decoder strategies for achieving low error floors," in *Proc. Inform. Theory Appl. Workshop*, San Diego, CA, USA, Jan. 2008, pp. 277–286.
- [3] Y. Zhang and W. E. Ryan, "Toward low LDPC-code floors: a case study," *IEEE Trans. Commun.*, vol. 57, no. 6, pp. 1566–1573, Jun. 2009.
- [4] G. B. Kyung and C.-C. Wang, "Finding the exhaustive list of small fully absorbing sets and designing the corresponding low error-floor decoder," *IEEE Trans. Commun.*, vol. 60, no. 6, pp. 1487–1498, Jun. 2012.
- [5] S. Zhang and C. Schlegel, "Controlling the error floor in LDPC decoding," *IEEE Trans. Commun.*, vol. 61, no. 9, pp. 3566–3575, Sep. 2013.
- [6] S. Tolouei and A. H. Banihashemi, "Lowering the error floor of LDPC codes using multi-step quantization," *IEEE Commun. Lett.*, vol. 18, no. 1, pp. 86–89, Jan. 2014.
- [7] X. Zhang and P. H. Siegel, "Quantized iterative message passing decoders with low error floor for LDPC codes," *IEEE Trans. Commun.*, vol. 62, no. 1, pp. 1–14, January 2014.
- [8] S. Kang, J. Moon, J. Ha and J. Shin, "Breaking the trapping sets in LDPC codes: Check node removal and collaborative decoding," *IEEE Trans. Commun.*, vol. 64, no. 1, pp. 15–26, Jan. 2016.
- [9] H.-C. Lee, P.-C. Chou and Y.-L. Ueng, "An effective low-complexity error-floor lowering technique for high-rate QC-LDPC codes," *IEEE Commun. Lett.*, vol. 22, no. 10, pp. 1988–1991, Oct. 2018.
- [10] H. Hatami, D. G. M. Mitchell, D. J. Costello and T. E. Fuja, "A threshold-based min-sum algorithm to lower the error floors of quantized LDPC decoders," *IEEE Trans. Commun.*, vol. 68, no. 4, pp. 2005–2015, Apr. 2020.
- [11] J. Zhao, F. Zarkeshvari and A. H. Banihashemi, "On implementation of min-sum algorithm and its modifications for decoding low-density parity-check (LDPC) codes," *IEEE Trans. Commun.*, vol. 53, no. 4, pp. 549–554, Apr. 2005.
- [12] Y. Mao and A. H. Banihashemi, "A heuristic search for good low-density parity-check codes at short block lengths," in *Proc. IEEE Int. Conf. Comm., Helsinki, Finland*, pp. 41–44, Jun. 2001.

- [13] T. Tian, C. Jones, J. D. Villasenor, and R. D. Wesel, "Selective avoidance of cycles in irregular LDPC code construction," *IEEE Trans. Commun.*, vol. 52, pp. 1242–1247, Aug. 2004.
- [14] H. Xiao and A. H. Banihashemi, "Improved progressive-edge-growth (PEG) construction of irregular LDPC codes," *IEEE Commun. Lett.*, vol. 8, no. 12, pp. 715–717, Dec. 2004.
- [15] X.-Y. Hu, E. Eleftheriou, and D.-M. Arnold, "Regular and irregular progressive edge-growth tanner graphs," *IEEE Trans. Inf. Theory*, vol. 51, no. 1, pp. 386–398, Jan. 2005.
- [16] M. Ivkovic, S. K. Chilappagari, and B. Vasic, "Eliminating trapping sets in low-density parity-check codes by using Tanner graph covers," *IEEE Trans. Inf. Theory*, vol. 54, no. 8, pp. 3763–3768, Aug. 2008.
- [17] X. Zheng, F. C.-M. Lau, and C. K. Tse, "Constructing short-length irregular LDPC codes with low error floor," *IEEE Trans. Commun.*, vol. 58, no. 10, pp. 2823–2834, Oct. 2010.
- [18] R. Asvadi, A. H. Banihashemi, and M. Ahmadian-Attari, "Lowering the error floor of LDPC codes using cyclic liftings," *IEEE Trans. Inf. Theory*, vol. 57, no. 4, pp. 2213–2224, Apr. 2011.
- [19] S. Khazraie, R. Asvadi and A. H. Banihashemi, "A PEG construction of finite-length LDPC codes with low error floor," *IEEE Commun. Lett.*, vol. 16, pp. 1288–1291, Aug. 2012.
- [20] D. V. Nguyen, S. K. Chilappagari, M. W. Marcellin, and B. Vasic, "On the construction of structured LDPC codes free of small trapping sets," *IEEE Trans. Inf. Theory*, vol. 58, no. 4, pp. 2280–2302, Apr. 2012.
- [21] X. Tao, Y. Li, Y. Liu, and Z. Hu, "On the construction of LDPC codes free of small trapping sets by controlling cycles," *IEEE Commun. Lett.*, vol. 22, no. 1, pp. 9–12, Jan. 2018.
- [22] S. Naseri and A. H. Banihashemi, "Construction of girth-8 QC-LDPC codes free of small trapping sets," *IEEE Commun. Lett.*, vol. 23, no. 11, pp. 1904–1908, Nov. 2019.
- [23] S. Naseri and A. H. Banihashemi, "Spatially coupled LDPC codes with small constraint length and low error floor," *IEEE Commun. Lett.*, vol. 24, no. 2, pp. 254–258, Feb. 2020.
- [24] B. Karimi and A. H. Banihashemi, "Construction of QC LDPC codes with low error floor by efficient systematic search and elimination of trapping sets," *IEEE Trans. Commun.*, vol. 68, no. 2, pp. 697–712, Feb. 2020.
- [25] B. Karimi and A. H. Banihashemi, "Construction of irregular protograph-based QC-LDPC codes with low error floor," *IEEE Trans. Commun.*, vol. 69, no. 1, pp. 3–18, Jan. 2021.
- [26] S. Naseri and A. H. Banihashemi, "Construction of time invariant spatially coupled LDPC codes free of small trapping sets," *IEEE Trans. Commun.*, available on IEEExplore Early Access.
- [27] C. C. Wang, S. R. Kulkarni, and H. V. Poor, "Finding all small error-prone substructures in LDPC codes," *IEEE Trans. Inf. Theory*, vol. 55, no. 5, pp. 1976–1999, May 2009.
- [28] M. Karimi and A. H. Banihashemi, "Efficient algorithm for finding dominant trapping sets of LDPC codes," *IEEE Trans. Inf. Theory*, vol. 58, no. 11, pp. 6942–6958, Nov. 2012.
- [29] M. Karimi and A. H. Banihashemi, "On characterization of elementary trapping sets of variable-regular LDPC codes," *IEEE Trans. Inf. Theory*, vol. 60, no. 9, pp. 5188–5203, Sep 2014.
- [30] Y. Hashemi and A. Banihashemi, "On characterization and efficient exhaustive search of elementary trapping sets of variable-regular LDPC codes," *IEEE Commun. Lett.*, vol. 19, pp. 323–326, Mar. 2015.
- [31] Y. Hashemi and A. H. Banihashemi, "New characterization and efficient exhaustive search algorithm for leafless elementary trapping sets of variable-regular LDPC codes," *IEEE Trans. Inf. Theory*, vol. 62, no. 12, pp. 6713–6736, Dec. 2016.
- [32] Y. Hashemi and A. H. Banihashemi, "Characterization of elementary trapping sets in irregular LDPC codes and the corresponding efficient exhaustive search algorithms," *IEEE Trans. Inf. Theory*, vol. 64, no. 5, pp. 3411–3430, May 2018.
- [33] T. Richardson, "Error floors of LDPC codes," in *Proc. 41th annual Allerton conf. on commun. control and computing*, Monticello, IL, USA, Oct. 2003, pp. 1426–1435.

- [34] J. Sun, "Studies on graph-based coding systems," Ph.D. dissertation, Dept. Elect. Eng., Ohio State Univ., Columbus, OH, USA, 2004.
- [35] C. A. Cole, S. G. Wilson, E. K. Hall, and T. R. Giallorenzi, "A general method for finding low error rates of LDPC codes," *submitted to IEEE Trans. Inf. Theory*, May 2006.
- [36] L. Dolecek, Z. Zhang, M. Wainwright, V. Anatharam, and B. Nikolic. "Evaluation of the low frame error rate performance of LDPC codes using importance sampling," in *Proc. IEEE Inf. Theory Workshop*, Lake Tahoe, CA, Sep. 2–6, 2007, pp. 202–207.
- [37] H. Xiao and A. H. Banihashemi, "Estimation of bit and frame error rates of finite-length low-density parity-check codes on binary symmetric channels," *IEEE Trans. Commun.*, vol. 55, no. 12, pp. 2234–2239, Dec. 2007.
- [38] E. Cavus, C. L. Haymes and B. Daneshrad, "Low BER performance estimation of LDPC codes via application of importance sampling to trapping sets," *IEEE Trans. Commun.*, vol. 57, no. 7, pp. 1886–1888, Jul. 2009.
- [39] L. Dolecek, P. Lee, Z. Zhang, V. Anatharam, B. Nikolic, and M. J. Wainwright, "Predicting error floors of structured LDPC codes: deterministic bounds and estimates," *IEEE J. Sel. Areas Commun.*, vol. 27, no. 6, pp. 908–917, Aug. 2009.
- [40] B. Vasić, S. K. Chilappagari, D. V. Nguyen and S. K. Planjery, "Trapping set ontology," in *Proc. 47th Allerton Conf.*, Monticello, IL, 2009, pp. 1–7.
- [41] X. Hu, Z. Li, B. Kumar, and R. Barndt, "Error floor estimation of long LDPC codes on magnetic recording channels," *IEEE Trans. Magn.*, vol. 46, no. 6, pp. 1836–1839, Jun. 2010.
- [42] C. Schlegel and S. Zhang, "On the dynamics of the error floor behavior in (regular) LDPC codes," *IEEE Trans. Inf. Theory*, vol. 56, no. 7, pp. 3248–3264, Jul. 2010.
- [43] H. Xiao, A. H. Banihashemi, and M. Karimi, "Error rate estimation of low-density parity-check codes decoded by quantized soft-decision iterative algorithms," *IEEE Trans. Commun.*, vol. 61, no. 2, pp. 474–484, Feb. 2013.
- [44] S. Tolouei and A. H. Banihashemi, "Fast and accurate error floor estimation of quantized iterative decoders for variable-regular LDPC codes," *IEEE Comm. Lett.*, vol. 18, no. 8, pp. 1283–1286, Aug. 2014.
- [45] B. K. Butler and P. H. Siegel, "error floor approximation for LDPC codes in the AWGN channel," *IEEE Trans. Inf. Theory*, vol. 60, no. 12, pp. 7416–7441, Dec. 2014.
- [46] H. Hatami, D. G. M. Mitchell, D. J. Costello and T. E. Fuja, "Performance bounds and estimates for quantized LDPC decoders," *IEEE Trans. Commun.*, vol. 68, no. 2, pp. 683–696, Feb. 2020.
- [47] A. Farsiabi and A. H. Banihashemi, "Error floor estimation of LDPC decoders - A code independent approach to measuring the harmfulness of trapping sets," *IEEE Trans. Commun.*, vol. 68, no. 5, pp. 2667–2679, May 2020.
- [48] N. Raveendran, D. Declercq and B. Vasic, "A sub-graph expansion-contraction method for error floor computation," *IEEE Trans. Commun.*, vol. 68, no. 7, pp. 3984–3995, July 2020.
- [49] M. Zhu, M. Jiang and C. Zhao, "Error floor estimation of QC-LDPC coded modulation with importance sampling," *IEEE Comm. Lett.*, vol. 25, no. 1, pp. 28–32, Jan. 2021.
- [50] P. Neshaastegaran, A. H. Banihashemi and R. Gohary, "Error floor estimation of LDPC coded modulation systems using importance sampling," *IEEE Trans. Commun.*, available in IEEEExplore Early Access.
- [51] A. Tomasoni, S. Bellini and M. Ferrari, "Thresholds of absorbing sets in low-density parity-check codes," *IEEE Trans. Commun.*, vol. 65, no. 8, pp. 3238–3249, Aug. 2017.
- [52] T. J. Richardson, M. A. Shokrollahi and R. L. Urbanke, "Design of capacity-approaching irregular low-density parity-check codes," *IEEE Trans. Inf. Theory*, vol. 47, no. 2, pp. 619–637, Feb 2001.
- [53] O. Milenkovic, E. Soljanin, and P. Whiting, "Asymptotic spectra of trapping sets in regular and irregular LDPC code ensembles," *IEEE Trans. Inf. Theory*, vol. 53, no. 1, pp. 39–55, Jan. 2007.

- [54] M. Mansour, N. Shanbhag, "High-throughput LDPC decoders," *IEEE Trans. Very Large Scale Integr. (VLSI) Syst.*, vol. 11, no. 6, pp. 976–996, Dec. 2003.
- [55] D. Hocevar, "A reduced complexity decoder architecture via layered decoding of LDPC codes," in *Proc. IEEE Workshop Signal Processing and Systems (SIPS.04)*, Austin, TX, Oct. 2004, pp. 107–112.
- [56] H. Xiao and A. H. Banihashemi, "Graph-based message-passing schedules for decoding LDPC codes," *IEEE Trans. Commun.*, vol. 52, no. 12, pp. 2098–2105, Dec. 2004.
- [57] A. Nough and A. H. Banihashemi, "Reliability-based schedule for bit-flipping decoding of low-density parity-check codes," *IEEE Trans. Commun.*, vol. 52, no. 12, pp. 2038–2040, Dec. 2004.
- [58] T. Brack, M. Alles, F. Kienle, N. Wehn, "A synthesizable IP core for WiMAX 802.16e LDPC code decoding," in *Proc. IEEE 17th Int. Symp. Personal Indoor and Mobile Radio Communications*, Sept. 2006, pp. 1–5.
- [59] Z. Wang, Z. Cui, "Low-complexity high-speed decoder design for quasi-cyclic LDPC codes," *IEEE Trans. VLSI Syst.*, vol. 15, no. 1, pp. 104–114, Jan. 2007.
- [60] K. Gunnam, G. Choi, M. Yearly, M. Atiquzzaman, "VLSI architectures for layered decoding for irregular LDPC codes of WiMax," in *Proc. IEEE Int. Conf. Commun. (ICC)*, June 2007, pp. 4542–4547.
- [61] E. Sharon, S. Litsyn, J. Goldberger, "Efficient serial message-passing schedules for LDPC decoding," *IEEE Trans. Inf. Theory*, vol. 53, no. 11, pp. 4076–4091, Nov. 2007.
- [62] C.-H. Liu, S.-W. Yen, C.-L. Chen, H.-C. Chang, C.-Y. Lee, Y.-S. Hsu, S.-J. Jou, "An LDPC decoder chip based on self-routing network for IEEE 802.16e applications," *IEEE J. Solid-State Circuits*, vol. 43, no. 3, pp. 684–694, March 2008.
- [63] K. Zhang, X. Huang and Z. Wang, "High-throughput layered decoder implementation for quasi-cyclic LDPC codes," *IEEE J. Sel. Areas Commun.*, vol. 27, no. 6, pp. 985–994, August 2009.
- [64] Z. Cui, Z. Wang, X. Zhang, "Reduced-complexity column-layered decoding and implementation for LDPC codes," *IET Commun.*, vol. 5, no. 15, pp. 2177–2186, 2011.
- [65] A. I. V. Casado, M. Griot and R. D. Wesel, "LDPC decoders with informed dynamic scheduling," *IEEE Trans. Commun.*, vol. 58, no. 12, pp. 3470–3479, December 2010.
- [66] H. Lee and Y. Ueng, "LDPC decoding scheduling for faster convergence and lower error floor," *IEEE Trans. Commun.*, vol. 62, no. 9, pp. 3104–3113, Sept. 2014.
- [67] N. Raveendran and B. Vasic, "Trapping set analysis of horizontal layered decoder," in *Proc. Int. Conf. Commun. (ICC)*, Kansas City, MO, 2018, pp. 1–6.
- [68] F. Angarita, J. Valls, V. Almenar and V. Torres, "Reduced-complexity min-sum algorithm for decoding LDPC codes with low error-floor," *IEEE Trans. Circuits Syst. I*, vol. 61, no. 7, pp. 2150–2158, July 2014.
- [69] X. Chen, J. Kang, S. Lin and V. Akella, "Hardware implementation of a backtracking-based reconfigurable decoder for lowering the error floor of quasi-cyclic LDPC codes," *IEEE Trans. Circuits Syst. I*, vol. 58, no. 12, pp. 2931–2943, Dec. 2011.
- [70] S. Kim, "Trapping set error correction through adaptive informed dynamic scheduling decoding of LDPC codes," *IEEE Commun. Lett.*, vol. 16, no. 7, pp. 1103–1105, July 2012.
- [71] B. K. Butler and P. H. Siegel, "Numerical issues affecting LDPC error floors," in *Proc. IEEE Global Telecommun. Conf.*, Anaheim, CA, 2012, pp. 3201–3207.
- [72] C. D. Meyer, *Matrix Analysis and Applied Linear Algebra*. Philadelphia, PA, USA: SIAM, 2000.
- [73] R. S. Varga, *Matrix Iterative Analysis*, 2nd ed, Berlin: Springer, 2000.
- [74] D. Noutsos, "Perron-Frobenius theory and some extensions", Como, Italy, May 2008, [Presentation Slides]. Available: <http://www.math.uoi.gr/~dnoutsos/Papers-pdf-files/slide-perron.pdf>.

- [75] R. A. Horn, C. R. Johnson, *Matrix Analysis*, Cambridge, U.K.: Cambridge Univ. Press, 1985.
- [76] *IEEE Standard for Local and Metropolitan Area Networks—Part 16: Air Interface for Fixed and Mobile Broadband Wireless Access Systems Amendment 2: Physical and Medium Access Control Layers for Combined Fixed and Mobile Operation in Licensed Bands and Corrigendum 1*, IEEE Standard 802.16e-2005 and 802.16-2004/Cor 1-2005, Feb. 2006.
- [77] A. Farsiabi, “Code-independent error floor estimation techniques for flooding and layered decoders of LDPC codes,” Ph.D. dissertation, Dept. of Systems and Computer Engineering, Carleton Univ., Ottawa, ON, Canada, 2020.
- [78] A. Farsiabi and A. H. Banihashemi, “Error floor analysis of column layered decoders,” to be submitted to *IEEE Trans. Commun.*.